

Two-particle Berry phase mechanism for Dirac and Majorana Kramers pairs of corner modes

Yi Tan,^{1,2,*} Zhi-Hao Huang,^{1,2,*} and Xiong-Jun Liu^{1,2,3,4,†}

¹*International Center for Quantum Materials and School of Physics, Peking University, Beijing 100871, China*

²*Collaborative Innovation Center of Quantum Matter, Beijing 100871, China*

³*CAS Center for Excellence in Topological Quantum Computation,
University of Chinese Academy of Sciences, Beijing 100190, China*

⁴*Institute for Quantum Science and Engineering and Department of Physics,
Southern University of Science and Technology, Shenzhen 518055, China*

We uncover a novel two-particle Berry phase mechanism to realize exotic corner modes in second-order topological insulators (TIs) and topological superconductors (TSCs) with time-reversal symmetry. We show that the nontrivial pseudospin textures of edge states in two different types of two-dimensional TIs give rise to the novel two-particle geometric phases in the particle-hole and particle-particle channels, respectively, for which the edge mass domain walls or intrinsic π -junctions emerge across corners when an external magnetic field or s -wave superconductivity is considered, hosting Dirac or Majorana corner modes. Remarkably, with this mechanism we predict the Majorana Kramers pair of corner modes by directly coupling the edge of a type-II time-reversal invariant TI to a uniform s -wave SC, in sharp contrast to the previous proposals which rely on unconventional SC pairing or complex setting for fine-tuned SC π -junction. We find Au/GaAs(111) to be a realistic material candidate for realizing such Majorana Kramers pair of corner modes.

Introduction.— Topological phases have generated great interest in the past decades [1–3]. Recently, the higher-order topological insulators (TIs) and topological superconductors (TSCs) were proposed [4–10]. An n th-order TI (TSC) in d dimension (dD) features topologically protected gapless states on its $(d - n)D$ boundary, but is gapped elsewhere. For example, a 2D second-order topological insulator (SOTI) hosts in-gap modes at the corners, while its both 2D bulk and 1D edges are gapped [2, 16]. The physics of corner modes is readily understood from the perspective of Dirac equations: The original helical edge states of a 2D time-reversal (TR) invariant TI are gapped by a sign-changing Dirac mass, leading to the corner modes at the mass domain walls [11–13]. The same picture applies to the case of 2D second-order topological superconductors (SOTSCs).

While the interests grow rapidly on the higher-order topological phases, the experimental realization of such phases in solid materials is rare, albeit various interesting theoretical schemes have been proposed [1, 2, 8, 14–19, 22, 23]. In comparison with higher-order topological insulators, the superconducting counterparts are usually even more demanding in the realization [24–32]. In particular, for the second-order time-reversal (TR) invariant TSCs which host Majorana Kramers pairs (MKPs) of corner modes, the existing proposals rely on either the coupling of TI helical edge states to unconventional superconductivity [33, 34] or complex settings for fine-tuned SC π -junctions [35–37]. The MKPs obey the symmetry-protected non-Abelian statistics, manifesting a new type of non-Abelian anyons [38–44]. Thus to uncover experimental schemes, albeit being currently very scarce [45], to realize the MKPs is highly significant and of broad interests.

In this Letter, we propose a fundamental mechanism by introducing a novel concept of two-particle Berry phase to characterize and realize topological corner modes in second-order topological phases. We show that two different scenarios of Berry phases arise from the pseudospin textures of

edge states [46] in two different types of 2D TIs, leading to the sign changes in the gap opened at edge and across corners when external magnetic field or superconductivity is applied. In the SOTI phase, the mass domain wall emerges and originates from the two-particle Berry phase of particle-hole channel, leading to the transition from QSH to SOTI phase by applying a uniform in-plane magnetic field. In the SOTSC phase, *intrinsic* π -junctions emerge at corners and are resulted from the two-particle Berry phases of particle-particle channel (Cooper pair), giving rise to MKPs of corner modes with TR symmetry. Remarkably, with this mechanism we predict that the MKPs can be realized by directly superposing a type-II TI on a uniform s -wave SC, in sharp contrast to the previous proposals [33–37]. This prediction updates a traditional viewpoint that, due to the TR symmetry, a uniform s -wave proximate SC can induce a uniform pairing order without node in and thus fully gap out the helical edge states of TI, see e.g. refs [47, 48]. Our finding shows that for a broad class of the quantum spin-Hall insulators, the intrinsic π -junction emerges across corners when the edge is coupled to a uniform s -wave SC, leading to the MKPs of corner modes. We show the QSH insulator Au/GaAs(111) thin film [3, 49] as a 2D material candidate for the realization of the MKPs, and further provide a generic guideline in searching for such SOTSC phases.

The generic edge theory.—We start with a generic edge theory of the geometric phase mechanism for corner modes. The theory is extended from a previous result that the chiral edge state in a class of quantum anomalous Hall (QAH) insulators exhibits topological (pseudo)spin texture in real space, with the pseudospin polarization of each edge state winding one big circle along the closed 1D boundary in the presence of chiral symmetry [46, 51]. Such pseudospin texture defines a π Berry phase on the boundary. For a TR invariant TI formed by two copies of QAH insulators with opposite Chern numbers, its helical edge states form Kramers pairs of the TRS $\mathcal{T} = i s_y \mathcal{K}$, with s_y being spin operator and \mathcal{K} the complex conju-

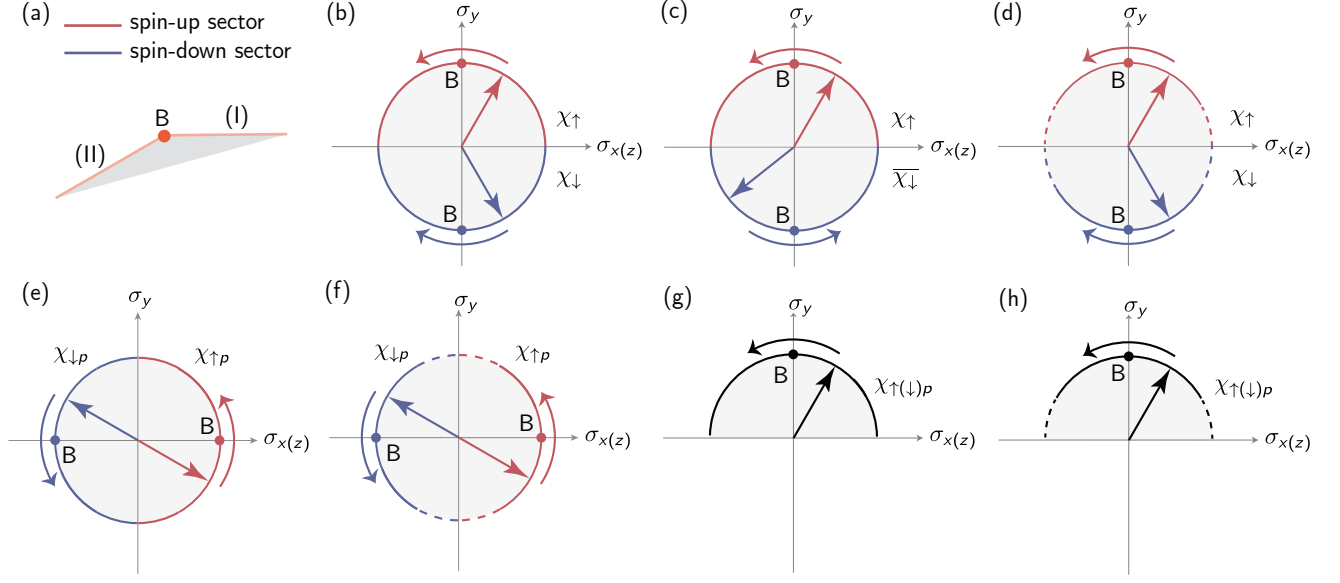


Figure 1. Boundary pseudospin textures of TIs crossing corner B. (a) Schematic plot of the adjacent edges in real space. (b) Pseudospin trajectories for $|\chi_{\uparrow}\rangle$ (red solid lines) and $|\chi_{\downarrow}\rangle$ (blue solid lines) wind oppositely in the intrinsic space. The straight red(blue) arrows denote the pseudospin vectors for $|\chi_{\uparrow}\rangle(|\chi_{\downarrow}\rangle)$. (c) The joint trajectory for $|\chi_{\uparrow}\rangle$ and $|\chi_{\downarrow}\rangle$ can be viewed as a closed loop in intrinsic space, which enables a well-defined two-state Berry phase in PH channel γ_{ph} , leading to the Dirac corner modes. (d) The conclusion in (c) also apply to the situation where pseudospin trajectories are non-closed and can be connected by the continuation trajectories (dashed lines). (e) and (g) The winding of pseudospin trajectories within both spin sectors are in the same direction. The straight black arrows represent the coinciding of pseudospin vectors for $|\chi_{\uparrow}\rangle$ and $|\chi_{\downarrow}\rangle$. And the two-state Berry phase in PP channel γ_{pp} is of importance since the joint trajectories for $|\chi_{\uparrow p}\rangle$ and $|\chi_{\downarrow p}\rangle$ are closed, guaranteeing the appearance of the MKPs. This result can be extended to non-closed cases (f) and (h).

gate. The pseudospin polarizations of spin-up ($|\chi_{\uparrow}\rangle$) and spin-down ($|\chi_{\downarrow}\rangle$) edge states are given by $\langle\sigma_{\uparrow}\rangle = \langle\chi_{\uparrow}|s_0\sigma|\chi_{\uparrow}\rangle$ and $\langle\sigma_{\downarrow}\rangle = \langle\chi_{\downarrow}|s_0\sigma|\chi_{\downarrow}\rangle$, where the pseudospin operators σ denote the orbital (or sublattice) degree of freedom. When traveling from one edge to a neighboring edge across a corner point B in the real space [Fig. 1(a)], the pseudospin direction ($\langle\sigma_{\uparrow,\downarrow}\rangle$) of a single state in general does not trace a closed loop. However, a *two-state Berry phase* can be defined when the pseudospin polarizations are inverted across the corner for both spin-up and spin-down sectors. Two basic cases corresponding two fundamental types of TIs are of particular interests and studied below.

First, the pseudospin trajectories of the two spin sectors wind oppositely, e.g. $(\langle\sigma_{\uparrow x}\rangle, \langle\sigma_{\uparrow y}\rangle) = (\langle\sigma_{\downarrow x}\rangle, -\langle\sigma_{\downarrow y}\rangle)$ [Fig. 1(b)], so the joint pseudospin trajectory of the spin-up particle and spin-down hole is closed in intrinsic space [Fig. 1(c)]. The case that TR symmetry reverses only real spin, but not pseudospin bases belongs to this scenario. We define the two-state Berry phase in particle-hole (PH) channel

$$\gamma_{ph} = \int_{\theta^{(I)}}^{\theta^{(II)}} d\theta \langle\chi_{\uparrow}(\theta)| \langle\chi_{\downarrow}(\theta)| (-i\partial_{\theta}) |\chi_{\uparrow}(\theta)\rangle \otimes |\chi_{\downarrow}(\theta)\rangle. \quad (1)$$

Here $\theta^{(I,II)}$ stands for the normal direction of edge I and II, and the spin-down hole state $|\chi_{\downarrow}\rangle$ is obtained by charge conjugation \mathcal{K} on $|\chi_{\uparrow}\rangle$, equivalent to flipping a ket into a bra state. Applying a uniform in-plane Zeeman field $(\mathbf{M} \cdot \mathbf{s})\sigma_0$

to break the TRS and introduce mass term $\mathcal{H}_{\text{mass}}$ [52] to the edge Dirac Hamiltonian $\mathcal{H}_{\text{edge}} = vk_{\parallel}s_z$ [2]. The matrix element $\langle\chi_{\uparrow}|(\mathbf{M} \cdot \mathbf{s})\sigma_0|\chi_{\downarrow}\rangle$ resembles a particle-hole excitation gap on the edge, and when turning from edge I to edge II across the corner point B, the mass term is related by [52]

$$\langle\chi_{\uparrow}^{(II)}|(\mathbf{M} \cdot \mathbf{s})\sigma_0|\chi_{\downarrow}^{(II)}\rangle = e^{-i\gamma_{ph}} \langle\chi_{\uparrow}^{(I)}|(\mathbf{M} \cdot \mathbf{s})\sigma_0|\chi_{\downarrow}^{(I)}\rangle. \quad (2)$$

Consequently, for $\gamma_{ph} = \pm\pi$ a mass domain wall is obtained across the corner, giving zero-energy corner modes. This result can be extended to the more generic configuration that the pseudospin polarization of each spin sector is not fully inverted across the corner [Fig. 1(d)]. In this case we consider a continuation [shown in dashed line of Fig. 1(d)] to connect them so that the two-state pseudospin trajectory is still closed and a two-state π Berry phase is resulted. As long as no node of mass is obtained on the continuation trajectories, the mass domain wall must be obtained across the corner. We note that the π Berry phase and zero-energy mode for the insulating phase necessitate protection by a chiral-like symmetry [52], which anticommutes with all terms in Hamiltonian. When this symmetry is broken, the pseudospin texture will not be fully in-plane and the Berry phase is no longer strictly quantized to π (even with closed pseudospin trajectories via continuation), hence not guaranteeing the full sign reversion of edge mass term. In this case the corner mode has finite energy but may still be within the gap if the Berry phase is close to π -value.

The second even more nontrivial case that we unveil is

the two-state Berry phase in the particle-particle (PP) channel, which corresponds to realizing MKPs of corner modes in SOTSCs when the edge is proximately coupled to a uniform s -wave SC. The case that TR symmetry reverses both real spin and pseudospin bases belongs to this scenario. Particularly, when the pseudospins of both spin sectors wind in the same direction across the corner, e.g. $(\langle\sigma_{\uparrow x}\rangle, \langle\sigma_{\uparrow y}\rangle) = \pm(\langle\sigma_{\downarrow x}\rangle, \langle\sigma_{\downarrow y}\rangle)$ [Fig. 1(e,g)], the two-state Berry phase in PH channel vanishes, but is nontrivial in PP channel

$$\gamma_{pp} = \int_{\theta^{(I)}}^{\theta^{(II)}} d\theta \langle\chi_{\uparrow p}(\theta)| \otimes \langle\chi_{\downarrow p}(\theta)| (-i\partial_{\theta}) |\chi_{\uparrow p}(\theta)\rangle \otimes |\chi_{\downarrow p}(\theta)\rangle. \quad (3)$$

For the edge Hamiltonian $\mathcal{H}_{\text{edge}} = ivk_{\parallel}\tau_y s_z$, the SC pairing term induced in the edge states reads $\mathcal{H}_{\text{mass}} = \langle\chi_{\uparrow p}|\Delta_s\tau_y s_y\sigma_0|\chi_{\downarrow h}\rangle\tau_y s_y$, where τ_y represents the particle-hole degree of freedom, and subscript p/h denotes the Nambu particle/hole sector. This matrix element gives the SC gap function in the edge and obeys [52]

$$\langle\chi_{\uparrow p}^{(II)}|\Delta_s\tau_y s_y\sigma_0|\chi_{\downarrow h}^{(II)}\rangle = e^{-i\gamma_{pp}} \langle\chi_{\uparrow p}^{(I)}|\Delta_s\tau_y s_y\sigma_0|\chi_{\downarrow h}^{(I)}\rangle. \quad (4)$$

In this case, a mass domain wall (an *intrinsic* π junction) is obtained when $\gamma_{pp} = \pm\pi$ and harbors at each corner a MKP, which obeys symmetry-protected non-Abelian statistics [38–44]. With the particle-hole symmetry being always present in superconductors, the MKPs of zero corner modes are protected by time-reversal symmetry, without the necessity of chiral-like symmetry in insulators. We emphasize that in this realization we directly superpose TI on a uniform and conventional s -wave SC, in sharp contrast to previous proposals of realizing MKPs of corner modes [33–37]. Again, this result does not require pseudospin to be fully inverted across the corner, as long as no node exists for the pairing order on the auxiliary trajectories [dashed lines in Fig. 1(f,h)].

Application to SOTSCs.—The edge two-particle Berry phase theory provides an intuitive principle to realize SO-TIs and SOTSCs, while we leave the discussion on SOTIs based on the first type of TI to the supplemental material [52], and hereby focus on the more nontrivial prediction of MKPs of corner modes. As required, we consider a generic type-II TI with two orbitals α and β transforming to each other under TRS, and propose two minimal-model realizations with such TI proximately coupled to an s -wave SC. The Hamiltonian in $\psi = (\psi_{\uparrow\alpha}, \psi_{\uparrow\beta}, \psi_{\downarrow\alpha}, \psi_{\downarrow\beta})^T$ basis is $H_{1(2)} = \int d\mathbf{k} \psi^\dagger(\mathbf{k})\mathcal{H}_{\text{TI-1(2)}}\psi(\mathbf{k}) + H_{s\text{-wave}}$, with $H_{s\text{-wave}} = \sum_{\sigma=\alpha,\beta} \int d\mathbf{k} \Delta_s(\psi_{\uparrow\sigma}(\mathbf{k})\psi_{\downarrow\sigma}(-\mathbf{k}) + \text{h.c.})$ being TR invariant, and the low-energy band Hamiltonian

$$\mathcal{H}_{\text{TI-1(2)}} = (m - t|\mathbf{k}|^2)s_z\sigma_z + vk_x s_{0(z)}\sigma_x + vk_y s_{0(z)}\sigma_y. \quad (5)$$

We consider square-shape boundary, with edges terminating the lattice in a tilted way [Fig. 2(a)]. When $\text{sgn } m \text{sgn } t > 0$, for an arbitrary sample edge with normal vector $\hat{\mathbf{x}}_{\perp} = (\cos\theta, \sin\theta)$, assuming a half-infinite sample area $x_{\perp} < 0$,

we can solve out the helical edge states

$$|\chi_{\uparrow}\rangle_{1,2} = \begin{bmatrix} 1 \\ 0 \end{bmatrix}_s \otimes \begin{bmatrix} \frac{1}{\sqrt{2}} \\ -\frac{ie^{i\theta}}{\sqrt{2}} \end{bmatrix}_{\sigma}, \quad |\chi_{\downarrow}\rangle_{1,2} = \begin{bmatrix} 0 \\ 1 \end{bmatrix} \otimes \begin{bmatrix} \frac{1}{\sqrt{2}} \\ \pm\frac{ie^{i\theta}}{\sqrt{2}} \end{bmatrix}_{\sigma} \quad (6)$$

Thus the pseudospin polarizations for $|\chi_{\uparrow,\downarrow}\rangle$ are $\langle\sigma_{\uparrow}\rangle_{1,2} = (\sin\theta, -\cos\theta, 0)$, $\langle\sigma_{\downarrow}\rangle_{1,2} = (\mp\sin\theta, \pm\cos\theta, 0)$. [Fig. 2(b)] We put here the numerical results for the first model, which is the case of the material candidate to be proposed later. The trajectories of two pseudospin polarizations across corner B (similar for other corners) are depicted as solid lines in Fig. 2(c), with in-between paths untraveled. So we can make a valid continuation [dashed lines in Fig. 2(c)] to concatenate the two trajectories, rendering a two-particle π Berry phase in the PP channel. According to the generic theory, a mass domain wall arises at the corner on the real trajectories if applying an s -wave SC, as shown in numerical results in Fig. 2(d). Note that the model has mirror symmetries. In particular, the mirror- x symmetry $\hat{M}_x = is_x\sigma_y\tau_z$ relates edges AB and BC, forcing a SC π -junction at intersection corner B, consistent with the Berry phase mechanism [52].

Realistic materials.—Now we propose the material realization of the above SOTSC. We focus on the Au/GaAs(111) thin film, which realizes QSH phase in triangular lattice [Fig. 3(a)] based on first-principle calculation [3]. The orbital compo-

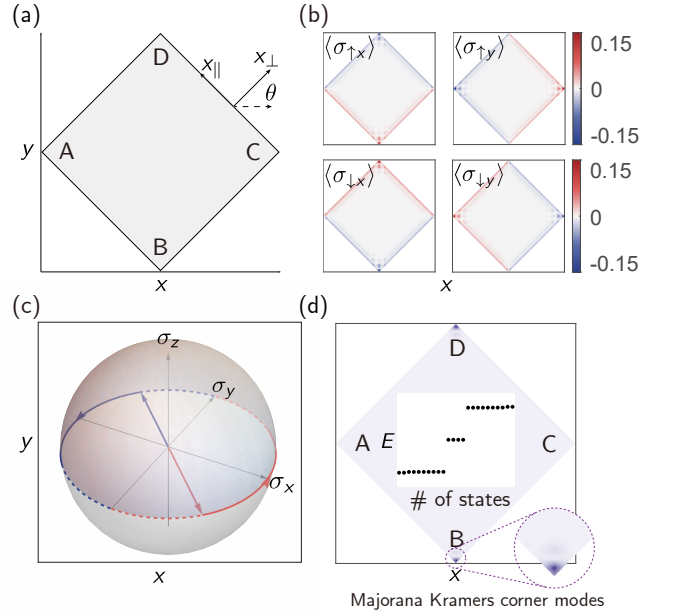


Figure 2. Pseudospin analysis for the first minimal model, with parameters $m = 2, t = 1, v = 1$. (a) Illustration of the sample geometry and normal vector of edges. (b) Numerical results of the pseudospin polarizations of the two spin sectors. (c) Trajectories of pseudospin polarizations of spin-up particle (red solid line) and spin-down particle (blue solid line) states traveling from edge AB to BC, with valid continuation (dashed lines). Concatenating two trajectories gives a complete winding which encircles 2π solid angle. (d) The distribution of the Dirac corner modes, and the energy level plotted under magnetic SC pairing strength $\Delta_s = 0.2$.

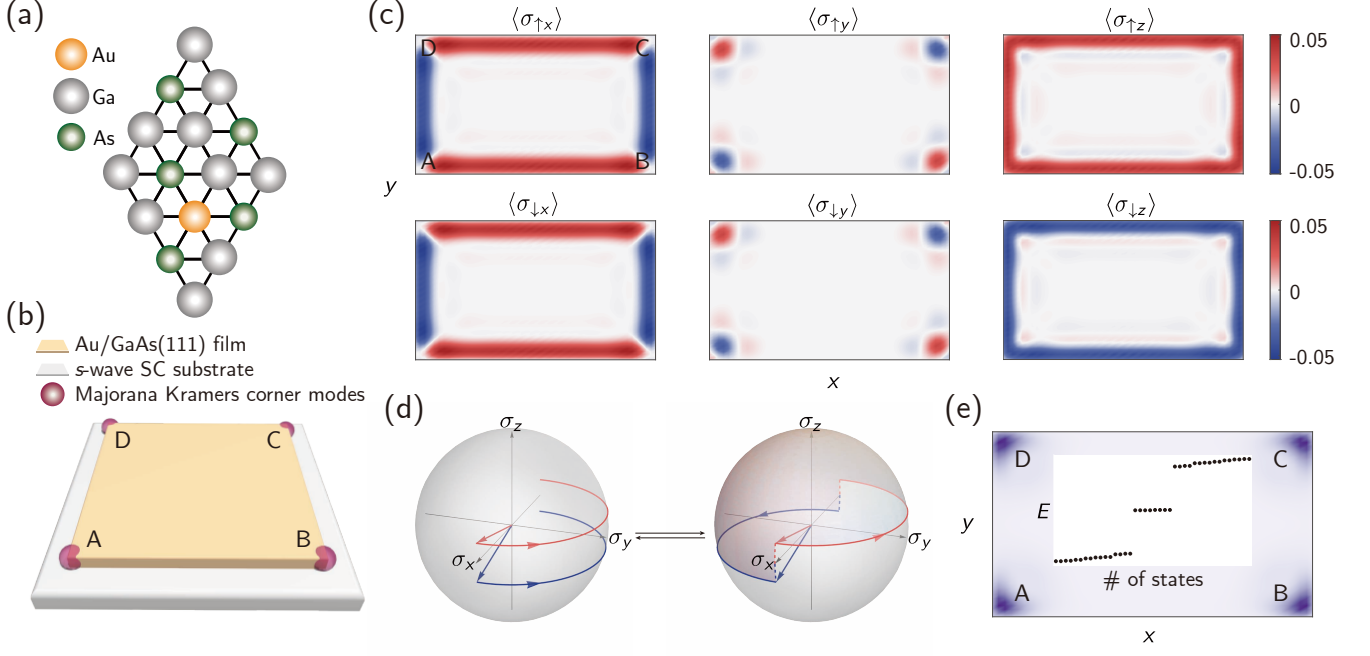


Figure 3. The material realization of SOTSC and its pseudospin analysis. (a) $\sqrt{3} \times \sqrt{3}R30^\circ$ trigonal superlattice of Au/GaAs(111) surface. (b) Schematic plot of the QSH/*s*-wave SC heterostructure with MKPs of corner modes. (c) Numerical results of the pseudospin polarizations. (d) Boundary pseudospin textures of the 2nd type QSH phase across corner B. Red and blue arcs are the real trajectories of pseudospin polarizations while dashed lines denote the continuation trajectories. (e) The distribution of MKPs and the energy levels. (c) and (e) are obtained with parameters $\varepsilon_s = 0.74\text{eV}$, $\varepsilon_p = 0\text{eV}$, $t_{ss\sigma} = -0.04\text{eV}$, $t_{sp\sigma} = 0.04\text{eV}$, $t_{pp\sigma} = 0.18\text{eV}$, $t_{pp\pi} = 0.005\text{eV}$, $\lambda = 0.06\text{eV}$, $\mu = 0.555\text{eV}$, $\Delta_s = 0.05\text{eV}$.

nents without SOC around Γ point are described by the sp^2 basis $(s, p_x + ip_y, p_x - ip_y)$, which captures the minimal model of the system. With SOC, two types of QSH phases are supported, respectively corresponding to *s*-*p* band inversion (the first type) and *p*-*p* gap-opening (the second type). In the following, we will study the second type QSH phase, whose effective Hamiltonian is obtained by eliminating the bottom *s* orbital from the original sp^2 orbitals [3]. The Hamiltonian of TI-SC heterostructure in $\psi = (p_{\uparrow+}, p_{\uparrow-}, p_{\downarrow+}, p_{\downarrow-})^T$ basis is $H = \int dk \psi^\dagger(\mathbf{k}) \mathcal{H}_{\text{eff}} \psi(\mathbf{k}) + H_{s\text{-wave}}$, with $H_{s\text{-wave}} = \sum_{\sigma=+,-} \int dk \Delta_s (p_{\uparrow\sigma}(\mathbf{k}) p_{\downarrow\sigma}(-\mathbf{k}) + \text{h.c.})$ and

$$\begin{aligned} \mathcal{H}_{\text{eff}}(\mathbf{k}) = & a_0 s_0 \sigma_0 + a'_0 (k_x^2 + k_y^2) s_0 \sigma_0 + \lambda s_z \sigma_z \\ & + a_x (k_x^2 - k_y^2) s_0 \sigma_x + a_y k_x k_y s_0 \sigma_y. \end{aligned} \quad (7)$$

As being required, here the TRS $\mathcal{T}'' = i s_y \sigma_x \mathcal{K}$ reverses both spin and orbitals [52], and the necessary pseudospin texture in generic theory is obtained. The pseudospin polarizations of an arbitrary edge read $\langle \sigma_{\uparrow} \rangle = (a_{\uparrow} \cos 2\theta, a_{\uparrow} \sin 2\theta, (1 - a_{\uparrow}^2)^{1/2})$, $\langle \sigma_{\downarrow} \rangle = (a_{\downarrow} \cos 2\theta, a_{\downarrow} \sin 2\theta, -(1 - a_{\downarrow}^2)^{1/2})$. It is easily verified that $a_{\uparrow} = a_{\downarrow} < 0$ [52], so pseudospin texture turns out to satisfy $(\langle \sigma_{\uparrow x} \rangle, \langle \sigma_{\uparrow y} \rangle) = (\langle \sigma_{\downarrow x} \rangle, \langle \sigma_{\downarrow y} \rangle)$, which gives the two-particle Berry phase in PP channel γ_{pp} . We further consider a rectangular sample proximate to the conventional *s*-wave SC [Fig. 3(b)]. When traveling across the corner B, the pseudospin trajectories [Fig. 3(c)] are depicted on the Bloch sphere [Fig. 3(d)]. The real trajectories of pseudospin polar-

izations of $|\chi_{\uparrow p}\rangle$ (red semicircle) and $|\chi_{\downarrow p}\rangle$ (blue semicircle) can be connected by the continuation (dashed lines) with no nodes of pairing order existing in the continuation trajectories. Thus the two-particle π -Berry phase in PP channel is obtained. Consequently, an intrinsic SC π -junction is resulted with a Majorana Kramer pair at the corner B, similar for the corners A, C and D. The numerical results of MKPs and energy spectrum [Fig. 3(e)] confirm our prediction. Also, an effective mirror symmetry $\hat{M}_{\hat{n}} = -i\tau_z s_z \sigma_z$ ($\hat{n} = \frac{\sqrt{2}}{2}\hat{x} + \frac{\sqrt{2}}{2}\hat{y}$) of the low-energy Hamiltonian can relate all adjacent edges, forcing the emergence of SC π junctions on every corner [52].

We note that our theory provides a generic guideline in search for realistic materials of the SOTSCs with MKPs via a uniform *s*-wave pairing and second type of TIs. In particular, in the type-II TI system the TRS reverses both the spin part and the orbital degree of freedom. Consequently, the TIs formed by *p*-*p* [53, 54], *p*-*d* [55–57], *d*-*d* [58, 59] orbitals satisfying this condition are candidates to realize the SOTSCs from uniform *s*-wave pairing.

Discussion and conclusion.— We have uncovered a new and fundamental mechanism by introducing a novel concept of two-particle edge Berry phase to characterize and realize second-order TIs or TSCs. Unlike other basic mechanisms like Wilson loop and topological multipole invariants in the bulk, the boundary two-particle Berry phase mechanism provides a fundamental and intuitive principle which facilitates to uncover new high-order topological matter. As concrete

examples of the application, we have predicted an unprecedented result that the Majorana Kramers pairs of corner modes are realized by directly coupling type-II TR invariant TI edge to a uniform s -wave SC, which stands in sharp contrast to the previous proposals. We further predicted the Au/GaAs(111) film as a material candidate for realization of the SOTSC, and a generic class of candidate materials are also discussed. Our prediction with new novel concept shall inspire further theoretical and experimental studies, including also the extension of the present study to higher dimensions.

Acknowledgments.—This work was supported by the National Key R&D Program of China (Grant No. 2021YFA1400900), National Natural Science Foundation of China (No. 11825401 and 11921005), and the Strategic Priority Research Program of Chinese Academy of Science (Grant No. XDB28000000).

* YT and ZHH contribute equally to this work.

† Corresponding author: xiongjunliu@pku.edu.cn.

- [1] M. Z. Hasan and C. L. Kane, *Rev. Mod. Phys.* **82**, 3045 (2010).
- [2] X.-L. Qi and S.-C. Zhang, *Rev. Mod. Phys.* **83**, 1057 (2011).
- [3] A. Bansil, H. Lin, and T. Das, *Rev. Mod. Phys.* **88**, 021004 (2016).
- [4] W. A. Benalcazar, B. A. Bernevig, and T. L. Hughes, *Science* **357**, 61 (2017).
- [5] W. A. Benalcazar, B. A. Bernevig, and T. L. Hughes, *Phys. Rev. B* **96**, 245115 (2017).
- [6] J. Langbehn, Y. Peng, L. Trifunovic, F. von Oppen, and P. W. Brouwer, *Phys. Rev. Lett.* **119**, 246401 (2017).
- [7] Z. Song, Z. Fang, and C. Fang, *Phys. Rev. Lett.* **119**, 246402 (2017).
- [8] F. Schindler, A. M. Cook, M. G. Vergniory, Z. Wang, S. S. P. Parkin, B. A. Bernevig, and T. Neupert, *Sci. Adv.* **4** (2018).
- [9] M. Geier, L. Trifunovic, M. Hoskam, and P. W. Brouwer, *Phys. Rev. B* **97**, 205135 (2018).
- [10] G. van Miert and C. Ortix, *Phys. Rev. B* **98**, 081110(R) (2018).
- [11] R. Jackiw and C. Rebbi, *Phys. Rev. D* **13**, 3398 (1976).
- [12] D. Čalugăru, V. Juričić, and B. Roy, *Phys. Rev. B* **99**, 041301 (2019).
- [13] F. Schindler, *Journal of Applied Physics* **128**, 221102 (2020).
- [14] M. Ezawa, *Phys. Rev. B* **98**, 045125 (2018).
- [15] F. Liu, H.Y. Deng, and K. Wakabayashi, *Phys. Rev. Lett.* **122**, 086804 (2019).
- [16] X.-L. Sheng, C. Chen, H. Liu, Z. Chen, Z.-M. Yu, Y. X. Zhao, and S. A. Yang, *Phys. Rev. Lett.* **123**, 256402 (2019).
- [17] B. Liu, G. Zhao, Z. Liu, and Z. F. Wang, *Nano Lett.* **19**, 6492 (2019).
- [18] E. Lee, R. Kim, J. Ahn, and B.-J. Yang, *npj Quantum Mater.* **5**, 1 (2020).
- [19] C. Chen, W. Wu, Z.-M. Yu, Z. Chen, Y. X. Zhao, X.-L. Sheng, S. A. Yang, arXiv: 2011.14868.
- [20] Y. Ren, Z. Qiao, and Q. Niu, *Phys. Rev. Lett.* **124**, 166804 (2020).
- [21] C. Chen, Z. Song, J.-Z. Zhao, Z. Chen, Z.-M. Yu, X.-L. Sheng, and S. A. Yang, *Phys. Rev. Lett.* **125**, 056402 (2020).
- [22] F. Liu and K. Wakabayashi, *Phys. Rev. Research* **3**, 023121 (2021).
- [23] B. Liu, L. Xian, H. Mu, G. Zhao, Z. Liu, A. Rubio, and Z.F. Wang, *Phys. Rev. Lett.* **126**, 066401 (2021).
- [24] T. Liu, J. J. He, and F. Nori, *Phys. Rev. B* **98**, 245413 (2018).
- [25] H. Shapourian, Y. Wang, and S. Ryu, *Phys. Rev. B* **97**, 094508 (2018).
- [26] Z. Yan, *Phys. Rev. Lett.* **123**, 177001 (2019).
- [27] X. Zhu, *Phys. Rev. Lett.* **122**, 236401 (2019).
- [28] Z. Wu, Z. Yan, and W. Huang, *Phys. Rev. B* **99**, 020508(R) (2019).
- [29] R.-X. Zhang, W. S. Cole, X. Wu, and S. Das Sarma, *Phys. Rev. Lett.* **123**, 167001 (2019).
- [30] Y. Peng and Y. Xu, *Phys. Rev. B* **99**, 195431 (2019).
- [31] X.-H. Pan, K.-J. Yang, L. Chen, G. Xu, C.-X. Liu, and X. Liu, *Phys. Rev. Lett.* **123**, 156801 (2019).
- [32] B. Roy, *Phys. Rev. B* **101**, 220506(R) (2020).
- [33] Q. Wang, C.-C. Liu, Y.-M. Lu, and F. Zhang, *Phys. Rev. Lett.* **121**, 186801 (2018).
- [34] Z. Yan, F. Song, and Z. Wang, *Phys. Rev. Lett.* **121**, 096803 (2018).
- [35] Y. Volpez, D. Loss, and J. Klinovaja, *Phys. Rev. Lett.* **122**, 126402 (2019).
- [36] C. Zeng, T.D. Stanescu, C. Zhang, V.W. Scarola, and S.Tewari, *Phys. Rev. Lett.* **123**, 060402 (2019).
- [37] K. Laubscher, D. Chughtai, D. Loss, and Je. Klinovaja, *Phys. Rev. B* **102**, 195401 (2020).
- [38] X.-J. Liu, C. L.M. Wong, and K.T.Law, *Phys. Rev. X* **4**, 021018 (2014).
- [39] K. Wölms, A. Stern, and K. Flensberg, *Phys. Rev. Lett.* **113**, 246401 (2014).
- [40] K. Wölms, A. Stern, and K. Flensberg, *Phys. Rev. B* **93**, 045417 (2016).
- [41] P. Gao, Y.-P. He, and X.-J. Liu, *Phys. Rev. B* **94**, 224509 (2016); *Phys. Rev. B* **95**, 019902 (2017).
- [42] A. Haim and Y. Oreg, *Physics Reports*, **825**, 1-48 (2019).
- [43] C. Knapp, A. Chew, and J. Alicea, *Phys. Rev. Lett.* **125**, 207002 (2020).
- [44] J.-S. Hong, T.-F. J. Poon, L. Zhang, and X.-J. Liu, *Phys. Rev. B* **105**, 024503 (2022).
- [45] Y. Zhang, K. Jiang, F. Zhang, J. Wang, and Z. Wang, *Phys. Rev. X* **11**, 011041 (2021).
- [46] J. Wu, J. Liu, and X.-J. Liu, *Phys. Rev. Lett.* **113**, 136403 (2014).
- [47] L. Fu and C. L. Kane, *Phys. Rev. B* **79**, 161408(R) (2009).
- [48] Jason Alicea, *Rep. Prog. Phys.* **75** 076501 (2012).
- [49] E. Hilner, A. Mikkelsen, J. Eriksson, J. N. Andersen, and E. Lundgren, *Appl. Phys. Lett.* **89**, 251912 (2006).
- [50] Z. F. Wang, K.-H. Jin, and F. Liu, *Nat Commun* **7**, 12746 (2016).
- [51] R.-X. Zhang, Hsiu-Chuan Hsu, and Chao-Xing Liu *Phys. Rev. B* **93**, 235315 (2016).
- [52] See Supplemental Material for details.
- [53] J. J. Zhou, W. Feng, C. C. Liu, S. Guan and Y. Yao, *Nano Lett.* **14**, 4767 (2014).
- [54] C. Li, K.-H. Jin, S. Zhang, F. Wang, Y. Jia and F. Liu, *Nanoscale* **10**, 5496 (2018).
- [55] X. Qian, J. Liu, L. Fu and J. Li, *Science* **346**, 1344 (2014).
- [56] M. Yang and W. M. Liu, *Sci Rep* **4**, 5131 (2014).
- [57] B. Huang, K. H. Jin, H. L. Zhuang, L. Zhang and F. Liu, *Phys. Rev. B* **93**, 115117 (2016).
- [58] H. Weng, A. Ranjbar, Y. Liang, Z. Song, M. Khazaei, S. Yunoki, M. Arai, Y. Kawazoe and X. Dai, *Phys. Rev. B* **92**, 075436 (2015).
- [59] C. Si, K. H. Jin, J. Zhou, Z. Sun and F. Liu, *Nano Lett.* **16**, 6584 (2016).

Supplementary Material

In this Supplemental Material, we derive the formalism for two-state Berry phases of particle-hole channel and particle-particle channel in detail and make a complementary discussion for the condition of the situation where no mass domain wall being induced in a corner turning process. Besides, we provide the details on the pseudospin analysis for the BHZ model and Kane-Mele model and the derivation of boundary pseudospin textures of the Au/AsGa(111) film. We also provide the lattice symmetry analysis for the SOTIs and SOTSCs.

I. FORMALISM FOR TWO-STATE BERRY PHASE

A. Formalism for two-state Berry phase in HOTI: particle-hole channel

From an arbitrary edge I to its neighboring edge II, the evolution of spinors for pseudospin with the varying of boundary parameter $\theta^{(I)} \rightarrow \theta^{(II)}$ in the real space induces the evolution of spinors in the intrinsic space for pseudospin, which can be represented by rotation on Bloch sphere for normalized spinors. Suppose that the pseudospin vector of each spin sector always lies within $\sigma_x - \sigma_y$ plane of intrinsic space, its spinor can be generally represented as $|\chi_s(\alpha_s)\rangle = e^{-i\frac{\alpha_s}{2}s_0(\sigma_z - \sigma_0)}|\chi_s(0)\rangle$ ($s = \uparrow, \downarrow$). The two spinors $|\chi_s(\alpha_s)\rangle$ ($s = \uparrow, \downarrow$) are related by TRS $|\chi_\downarrow(\alpha_\downarrow)\rangle = \mathcal{T}|\chi_\uparrow(\alpha_\uparrow)\rangle$. For the case $\mathcal{T} = is_y\mathcal{K}$, the two pseudospin vectors wind along opposite directions as θ varies, and we have the relation $\alpha_\uparrow = -\alpha_\downarrow$. For spinors on edge I and II, we denote $|\chi_s^{(I,II)}\rangle = |\chi_s(\alpha_s^{(I,II)})\rangle$ and $\alpha_s^{(II)} - \alpha_s^{(I)} = \Delta\alpha_s$, so $|\chi_s^{(II)}\rangle = e^{-i\frac{\Delta\alpha_s}{2}s_0(\sigma_z - \sigma_0)}|\chi_s^{(I)}\rangle$. Now consider the case where the pseudospin polarization of each spin sector gets fully inverted when turning the corner, say, $\alpha_{\uparrow,\downarrow}^{(I)} = 0$ and $\alpha_{\uparrow,\downarrow}^{(II)} = \pm\pi$. As shown in Fig. S1(a), since the pseudospin trajectory of each spin sector is non-closed, the Berry phase for each particle state ($|\chi_\uparrow\rangle$ or $|\chi_\downarrow\rangle$) can't be well defined. Interestingly, we find the trajectories of pseudospin of spin-up sector and spin-down sector wind oppositely, which leads to that the joint pseudospin trajectory of the particle state $|\chi_\uparrow\rangle$ and hole state $\overline{|\chi_\downarrow\rangle}$ (obtained by applying a particle-hole transformation on $|\chi_\downarrow\rangle$) is closed (vice versa). Therefore it is reasonable to define a two-state Berry phase in particle-hole channel:

$$\gamma_{ph} = \int_{\theta^{(I)}}^{\theta^{(II)}} d\theta \langle \chi_\uparrow(\theta) | \otimes \overline{\langle \chi_\downarrow(\theta) |} (-i\partial_\theta) | \chi_\uparrow(\theta) \rangle \otimes \overline{|\chi_\downarrow(\theta)\rangle} \quad (S1)$$

Since θ is solely determined by $\alpha_{\uparrow(\downarrow)}$ in each spin sector, the formula can be reformulated as

$$\begin{aligned} \gamma_{ph} &= \int_{\theta^{(I)}}^{\theta^{(II)}} d\theta \langle \chi_\uparrow(\theta) | \otimes \overline{\langle \chi_\downarrow(\theta) |} (-i\partial_\theta) \overline{|\chi_\downarrow(\theta)\rangle} \otimes |\chi_\uparrow(\theta)\rangle \\ &= \int_{\theta^{(I)}}^{\theta^{(II)}} d\theta \langle \chi_\uparrow(\theta) | (-i\partial_\theta) | \chi_\uparrow(\theta) \rangle + \int_{\theta^{(I)}}^{\theta^{(II)}} d\theta \overline{\langle \chi_\downarrow(\theta) |} (-i\partial_\theta) \overline{|\chi_\downarrow(\theta)\rangle} \\ &= \int_0^\pi d\alpha_\uparrow \frac{d\theta}{d\alpha_\uparrow} \langle \chi_\uparrow(\theta(\alpha_\uparrow)) | (-i\partial_\theta) | \chi_\uparrow(\theta(\alpha_\uparrow)) \rangle + \int_0^{-\pi} d\alpha_\downarrow \frac{d\theta}{d\alpha_\downarrow} \overline{\langle \chi_\downarrow(\theta(\alpha_\downarrow)) |} (-i\partial_\theta) \overline{|\chi_\downarrow(\theta(\alpha_\downarrow))\rangle} \\ &= \int_0^\pi d\alpha_\uparrow \langle \chi_\uparrow(\theta(\alpha_\uparrow)) | (-i\frac{d\theta}{d\alpha_\uparrow}\partial_\theta) | \chi_\uparrow(\theta(\alpha_\uparrow)) \rangle + \int_0^{-\pi} d\alpha_\downarrow \overline{\langle \chi_\downarrow(\theta(\alpha_\downarrow)) |} (-i\frac{d\theta}{d\alpha_\downarrow}\partial_\theta) \overline{|\chi_\downarrow(\theta(\alpha_\downarrow))\rangle} \\ &= \int_0^\pi d\alpha_\uparrow \langle \chi_\uparrow(\alpha_\uparrow) | (-i\partial_{\alpha_\uparrow}) | \chi_\uparrow(\alpha_\uparrow) \rangle + \int_0^{-\pi} d\alpha_\downarrow \overline{\langle \chi_\downarrow(\alpha_\downarrow) |} (-i\partial_{\alpha_\downarrow}) \overline{|\chi_\downarrow(\alpha_\downarrow)\rangle} \\ &= \int_0^\pi d\alpha_\uparrow \langle \chi_\uparrow(\alpha_\uparrow) | (-i\partial_{\alpha_\uparrow}) | \chi_\uparrow(\alpha_\uparrow) \rangle - \int_0^{-\pi} d\alpha_\downarrow \langle \chi_\downarrow(\alpha_\downarrow) | (-i\partial_{\alpha_\downarrow}) | \chi_\downarrow(\alpha_\downarrow) \rangle \end{aligned} \quad (S2)$$

where $\overline{|\chi_\downarrow(\alpha_\downarrow)\rangle}$ represents the hole counterpart of $|\chi_\downarrow(\alpha_\downarrow)\rangle$, which is obtained by a particle-hole transformation $\overline{|\chi_s(\alpha_s)\rangle} = e^{i\frac{\alpha_s}{2}s_0(\sigma_z - \sigma_0)}|\chi_s(0)\rangle$. When introducing an uniform in-plane magnetic field $(\mathbf{M} \cdot \mathbf{s})\sigma_0$, the mass term on an arbitrary edge is given by

$$\mathcal{H}_{\text{mass}}(\theta) = \begin{bmatrix} & \langle \chi_\uparrow(\theta) | (\mathbf{M} \cdot \mathbf{s}) \sigma_0 | \chi_\downarrow(\theta) \rangle \\ \langle \chi_\downarrow(\theta) | (\mathbf{M} \cdot \mathbf{s}) \sigma_0 | \chi_\uparrow(\theta) \rangle & \end{bmatrix} \quad (S3)$$

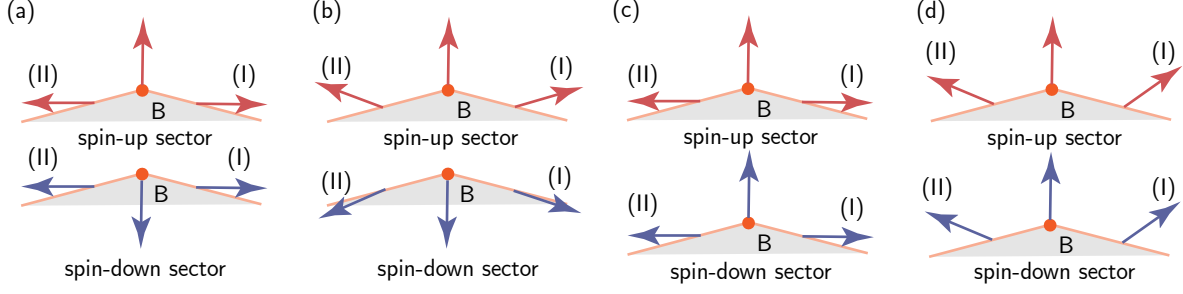


Figure S1. The pseudospin trajectories of both spin sectors across corner B. The pseudospin trajectories of spin-up and spin-down sectors in (a) and (b) wind oppositely, which allows a well-defined two-state Berry phase of particle-hole channel γ_{ph} . While in the (c) and (d), the windings of pseudospin trajectories of both spin sectors are in the same direction, leading to a vanished γ_{ph} and a nontrivial γ_{pp} .

We can derive the differential equation for the matrix element,

$$\begin{aligned}
& d\langle\chi_{\uparrow}(\theta(\alpha_{\uparrow}))|(\mathbf{M}\cdot\mathbf{s})\sigma_0|\chi_{\downarrow}(\theta(\alpha_{\downarrow}))\rangle \\
&= d\alpha_{\uparrow}\langle\partial_{\alpha_{\uparrow}}\chi_{\uparrow}(\alpha_{\uparrow})|(\mathbf{M}\cdot\mathbf{s})\sigma_0|\chi_{\downarrow}(\alpha_{\downarrow})\rangle + d\alpha_{\downarrow}\langle\chi_{\uparrow}(\alpha_{\uparrow})|(\mathbf{M}\cdot\mathbf{s})\sigma_0|\partial_{\alpha_{\downarrow}}\chi_{\downarrow}(\alpha_{\downarrow})\rangle \\
&= d\alpha_{\uparrow}\langle\partial_{\alpha_{\uparrow}}\chi_{\uparrow}(\alpha_{\uparrow})|\sum_s|\chi_s(\alpha_s)\rangle\langle\chi_s(\alpha_s)|(\mathbf{M}\cdot\mathbf{s})\sigma_0|\chi_{\downarrow}(\alpha_{\downarrow})\rangle + d\alpha_{\downarrow}\langle\chi_{\uparrow}(\alpha_{\uparrow})|(\mathbf{M}\cdot\mathbf{s})\sigma_0\sum_s|\chi_s(\alpha_s)\rangle\langle\chi_s(\alpha_s)|\partial_{\alpha_{\downarrow}}\chi_{\downarrow}(\alpha_{\downarrow})\rangle \\
&= (d\alpha_{\uparrow}\langle\partial_{\alpha_{\uparrow}}\chi_{\uparrow}(\alpha_{\uparrow})|\chi_{\uparrow}(\alpha_{\uparrow})\rangle + d\alpha_{\downarrow}\langle\chi_{\downarrow}(\alpha_{\downarrow})|\partial_{\alpha_{\downarrow}}\chi_{\downarrow}(\alpha_{\downarrow})\rangle)\langle\chi_{\uparrow}(\alpha_{\uparrow})|(\mathbf{M}\cdot\mathbf{s})\sigma_0|\chi_{\downarrow}(\alpha_{\downarrow})\rangle \\
&= -i\left[d\alpha_{\uparrow}\langle\chi_{\uparrow}(\alpha_{\uparrow})|(-i\partial_{\alpha_{\uparrow}})|\chi_{\uparrow}(\alpha_{\uparrow})\rangle + d\alpha_{\downarrow}\overline{\langle\chi_{\downarrow}(\alpha_{\downarrow})|(-i\partial_{\alpha_{\downarrow}})|\chi_{\downarrow}(\alpha_{\downarrow})\rangle}\right]\langle\chi_{\uparrow}(\alpha_{\uparrow})|(\mathbf{M}\cdot\mathbf{s})\sigma_0|\chi_{\downarrow}(\alpha_{\downarrow})\rangle, \tag{S4}
\end{aligned}$$

where we have used the relation $\langle\chi_{\downarrow}(\alpha_{\downarrow})|\partial_{\alpha_{\downarrow}}\chi_{\downarrow}(\alpha_{\downarrow})\rangle = -\overline{\langle\chi_{\downarrow}(\alpha_{\downarrow})|\partial_{\alpha_{\downarrow}}|\chi_{\downarrow}(\alpha_{\downarrow})\rangle}$. Integrating from edge I to edge II, we obtain $\langle\chi_{\uparrow}^{(II)}|(\mathbf{M}\cdot\mathbf{s})\sigma_0|\chi_{\downarrow}^{(II)}\rangle = e^{-i(\int_0^{\pi} d\alpha_{\uparrow}\langle\chi_{\uparrow}(\alpha_{\uparrow})|(-i\partial_{\alpha_{\uparrow}})|\chi_{\uparrow}(\alpha_{\uparrow})\rangle + \int_0^{-\pi} d\alpha_{\downarrow}\overline{\langle\chi_{\downarrow}(\alpha_{\downarrow})|(-i\partial_{\alpha_{\downarrow}})|\chi_{\downarrow}(\alpha_{\downarrow})\rangle})}\langle\chi_{\uparrow}^{(I)}|(\mathbf{M}\cdot\mathbf{s})\sigma_0|\chi_{\downarrow}^{(I)}\rangle = e^{-i\gamma_{ph}}\langle\chi_{\uparrow}^{(I)}|(\mathbf{M}\cdot\mathbf{s})\sigma_0|\chi_{\downarrow}^{(I)}\rangle$. The particle-hole channel two-state Berry phase γ_{ph} can be directly computed as follows,

$$\begin{aligned}
\gamma_{ph} &= -i\int_0^{\pi} d\alpha_{\uparrow}\langle\chi_{\uparrow}(\alpha_{\uparrow})|\partial_{\alpha_{\uparrow}}|\chi_{\uparrow}(\alpha_{\uparrow})\rangle - i\int_0^{-\pi} d\alpha_{\downarrow}\overline{\langle\chi_{\downarrow}(\alpha_{\downarrow})|\partial_{\alpha_{\downarrow}}|\chi_{\downarrow}(\alpha_{\downarrow})\rangle} \\
&= -i\int_0^{\pi} d\alpha_{\uparrow}\langle\chi_{\uparrow}(\alpha_{\uparrow})|\partial_{\alpha_{\uparrow}}|\chi_{\uparrow}(\alpha_{\uparrow})\rangle - i\int_0^{\pi} d(-\alpha_{\downarrow})\overline{\langle\chi_{\downarrow}(-\alpha_{\downarrow})|\partial_{(-\alpha_{\downarrow})}|\chi_{\downarrow}(-\alpha_{\downarrow})\rangle} \\
&= -i\int_0^{\pi} d\alpha_{\uparrow}\langle\chi_{\uparrow}(\alpha_{\uparrow})|\partial_{\alpha_{\uparrow}}|\chi_{\uparrow}(\alpha_{\uparrow})\rangle - i\int_{\pi}^{2\pi} d\alpha_{\uparrow}\langle\chi_{\uparrow}(\alpha_{\uparrow})|\partial_{\alpha_{\uparrow}}|\chi_{\uparrow}(\alpha_{\uparrow})\rangle \\
&= -i\int_0^{2\pi} d\alpha_{\uparrow}\langle\chi_{\uparrow}(\alpha_{\uparrow})|\partial_{\alpha_{\uparrow}}|\chi_{\uparrow}(\alpha_{\uparrow})\rangle \\
&= \pm\pi \pmod{2\pi}, \tag{S5}
\end{aligned}$$

where we have used the relation $\alpha_{\uparrow} = -\alpha_{\downarrow}$. Now it is readily seen that

$$\langle\chi_{\uparrow}^{(II)}|(\mathbf{M}\cdot\mathbf{s})\sigma_0|\chi_{\downarrow}^{(II)}\rangle = e^{-i\gamma_{ph}}\langle\chi_{\uparrow}^{(I)}|(\mathbf{M}\cdot\mathbf{s})\sigma_0|\chi_{\downarrow}^{(I)}\rangle = -\langle\chi_{\uparrow}^{(I)}|(\mathbf{M}\cdot\mathbf{s})\sigma_0|\chi_{\downarrow}^{(I)}\rangle. \tag{S6}$$

This result makes sure that a mass domain wall exists in the intersection of edge I and II and enables a Dirac corner mode. In fact, the joint pseudospin trajectories of $|\chi_{\uparrow}\rangle$ and $|\chi_{\downarrow}\rangle$ are usually non-closed [Fig. S1(b)], but we can always connect them by the way of continuation to obtain a closed loop on which the particle-hole channel two-state Berry phase is well defined. And we need to determine whether the mass term changes sign when traveling from edge I to edge II or not. We claim that there must be a mass domain wall at corner B as long as one can find the continuation trajectories in which no mass nodes exist.

B. Formalism for two-state Berry phase in HOTSC: particle-particle channel

Now we proceed to discuss the geometric phase relevant in the formation of SOTSC, which is the two-state Berry phase in the particle-particle channel. Similarly, the pseudospin vector is given by $|\chi_{s\tau}(\alpha_{s\tau})\rangle = e^{-i\frac{\alpha_{s\tau}}{2}\tau_0s_0(\sigma_z - \sigma_0)}|\chi_{s\tau}(0)\rangle$ ($s = \uparrow, \downarrow$

; $\tau = p, h$). For the case the TRS operator is modified and the two spinors wind along the same direction as θ varies, we have $d\alpha_{\uparrow p}(\theta) = d\alpha_{\downarrow p}(\theta)$. For simplicity, we take $\alpha_{\uparrow p} = \alpha_{\downarrow p}$, the discussion for the cases where $\alpha_{\uparrow p} = \alpha_{\downarrow p} + \text{const.}$ can be discussed similarly. For two adjacent edges I and II, we denote $|\chi_{sp}^{(I,II)}\rangle = |\chi_{sp}(\alpha_{sp} = \alpha_s^{(I,II)})\rangle$, and we first consider the situation where the vectors of pseudospin get fully reversed when traveling from edge I to edge II [Fig. S1(c)], say, $\alpha_{\uparrow, \downarrow}^{(I)} = 0$ and $\alpha_{\uparrow, \downarrow}^{(II)} = \pi$. Remarkably, since the two pseudospins vectors within different spin sectors wind along the same direction across the corner, the two-state Berry phase vanishes in the particle-hole channel, while in a new channel (particle-particle channel) it comes into being. We define the two-state Berry phase in the particle-particle channel as

$$\begin{aligned}
\gamma_{pp} &= \int_{\theta^{(I)}}^{\theta^{(II)}} d\theta \langle \chi_{\uparrow p}(\theta) | \otimes \langle \chi_{\downarrow p}(\theta) | (-i\partial_\theta) | \chi_{\uparrow p}(\theta) \rangle \otimes | \chi_{\downarrow p}(\theta) \rangle \rangle \\
&= \int_{\theta^{(I)}}^{\theta^{(II)}} d\theta \langle \chi_{\uparrow p}(\theta) | (-i\partial_\theta) | \chi_{\uparrow p}(\theta) \rangle + \int_{\theta^{(I)}}^{\theta^{(II)}} d\theta \langle \chi_{\downarrow p}(\theta) | (-i\partial_\theta) | \chi_{\downarrow p}(\theta) \rangle \\
&= -i \int_{\theta^{(I)}}^{\theta^{(II)}} d\alpha_{\uparrow p} \frac{d\theta(\alpha_{\uparrow p})}{d\alpha_{\uparrow p}} \langle \chi_{\uparrow p}(\theta(\alpha_{\uparrow p})) | \partial_\theta | \chi_{\uparrow p}(\theta(\alpha_{\uparrow p})) \rangle - i \int_{\theta^{(I)}}^{\theta^{(II)}} d\alpha_{\downarrow p} \frac{d\theta(\alpha_{\downarrow p})}{d\alpha_{\downarrow p}} \langle \chi_{\downarrow p}(\theta(\alpha_{\downarrow p})) | \partial_\theta | \chi_{\downarrow p}(\theta(\alpha_{\downarrow p})) \rangle \\
&= -i \int_{\theta^{(I)}}^{\theta^{(II)}} d\alpha_{\uparrow p} \langle \chi_{\uparrow p}(\theta(\alpha_{\uparrow p})) | \frac{d\theta(\alpha_{\uparrow p})}{d\alpha_{\uparrow p}} \partial_\theta | \chi_{\uparrow p}(\theta(\alpha_{\uparrow p})) \rangle - i \int_{\theta^{(I)}}^{\theta^{(II)}} d\alpha_{\downarrow p} \langle \chi_{\downarrow p}(\theta(\alpha_{\downarrow p})) | \frac{d\theta(\alpha_{\downarrow p})}{d\alpha_{\downarrow p}} \partial_\theta | \chi_{\downarrow p}(\theta(\alpha_{\downarrow p})) \rangle \\
&= \int_0^\pi d\alpha_{\uparrow p} \langle \chi_{\uparrow p}(\alpha_{\uparrow p}) | (-i\partial_{\alpha_{\uparrow p}}) | \chi_{\uparrow p}(\alpha_{\uparrow p}) \rangle + \int_0^\pi d\alpha_{\downarrow p} \langle \chi_{\downarrow p}(\alpha_{\downarrow p}) | (-i\partial_{\alpha_{\downarrow p}}) | \chi_{\downarrow p}(\alpha_{\downarrow p}) \rangle. \tag{S7}
\end{aligned}$$

Since $|\chi_{sh}(\alpha_{sh})\rangle$ is obtained by a particle-hole transformation on $|\chi_{sp}(\alpha_{sp})\rangle$,

$$\begin{aligned}
|\chi_{sh}(\alpha_{sh})\rangle &= \hat{C}(|\chi_{sp}(\alpha_{sp})\rangle) \\
&= \tau_x \mathcal{K}(e^{-i\frac{\alpha_{sp}}{2}\tau_0 s_0(\sigma_z - \sigma_0)} |\chi_{sp}^{(I)}\rangle) \\
&= e^{i\frac{\alpha_{sp}}{2}\tau_0 s_0(\sigma_z - \sigma_0)} |\chi_{sh}^{(I)}\rangle, \tag{S8}
\end{aligned}$$

and $|\chi_{sh}(\alpha_{sh})\rangle$ can also be written as $e^{-i\frac{\alpha_{sh}}{2}\tau_0 s_0(\sigma_z - \sigma_0)} |\chi_{sh}^{(I)}\rangle$, we obtain the relation $\alpha_{sp} = -\alpha_{sh}$. When introducing the conventional s -wave SC pairing $-\Delta_s \tau_y s_y \sigma_0$, the mass term on an arbitrary edge is given by

$$\mathcal{H}_{\text{mass}}(\theta) = -\Delta_s \begin{bmatrix} & \langle \chi_{\downarrow p}(\theta) | \tau_y s_y \sigma_0 | \chi_{\downarrow h}(\theta) \rangle \\ \langle \chi_{\downarrow h}(\theta) | \tau_y s_y \sigma_0 | \chi_{\uparrow p}(\theta) \rangle & \langle \chi_{\uparrow p}(\theta) | \tau_y s_y \sigma_0 | \chi_{\uparrow h}(\theta) \rangle \end{bmatrix}. \tag{S9}$$

Now the matrix element $\langle \chi_{\uparrow p}(\theta) | \tau_y s_y \sigma_0 | \chi_{\downarrow h}(\theta) \rangle$ is not the edge particle-hole excitation gap as in the previous case, but is rather the edge SC gap created through two-particle (Cooper) pairing. We derive the differential equation for the matrix element

$$\begin{aligned}
& d\langle \chi_{\uparrow p}(\theta(\alpha_{\uparrow p})) | \tau_y s_y \sigma_0 | \chi_{\downarrow h}(\theta(\alpha_{\downarrow h})) \rangle \\
&= d\alpha_{\uparrow p} \langle \partial_{\alpha_{\uparrow p}} \chi_{\uparrow p}(\alpha_{\uparrow p}) | \tau_y s_y \sigma_0 | \chi_{\downarrow h}(\alpha_{\downarrow h}) \rangle + d\alpha_{\downarrow h} \langle \chi_{\uparrow p}(\alpha_{\uparrow p}) | \tau_y s_y \sigma_0 | \partial_{\alpha_{\downarrow h}} \chi_{\downarrow h}(\alpha_{\downarrow h}) \rangle \\
&= d\alpha_{\uparrow p} \langle \partial_{\alpha_{\uparrow p}} \chi_{\uparrow p}(\alpha_{\uparrow p}) | \sum_{s\tau} |\chi_{s\tau}(\alpha_{s\tau})\rangle \langle \chi_{s\tau}(\alpha_{s\tau}) | \tau_y s_y \sigma_0 | \chi_{\downarrow h}(\alpha_{\downarrow h}) \rangle + d\alpha_{\downarrow h} \langle \chi_{\uparrow p}(\alpha_{\uparrow p}) | \tau_y s_y \sigma_0 | \sum_{s\tau} |\chi_{s\tau}(\alpha_{s\tau})\rangle \langle \chi_{s\tau}(\alpha_{s\tau}) | \partial_{\alpha_{\downarrow h}} \chi_{\downarrow h}(\alpha_{\downarrow h}) \rangle \\
&= (d\alpha_{\uparrow p} \langle \partial_{\alpha_{\uparrow p}} \chi_{\uparrow p}(\alpha_{\uparrow p}) | \chi_{\uparrow p}(\alpha_{s\tau}) \rangle + d\alpha_{\downarrow h} \langle \chi_{\downarrow h}(\alpha_{\downarrow h}) | \partial_{\alpha_{\downarrow h}} \chi_{\downarrow h}(\alpha_{\downarrow h}) \rangle) \langle \chi_{s\tau}(\alpha_{s\tau}) | \tau_y s_y \sigma_0 | \chi_{\downarrow h}(\alpha_{\downarrow h}) \rangle \\
&= -i [(d\alpha_{\uparrow p} \langle \chi_{\uparrow p}(\alpha_{\uparrow p}) | (-i\partial_{\alpha_{\uparrow p}}) | \chi_{\uparrow p}(\alpha_{\uparrow p}) \rangle + d\alpha_{\downarrow p} \langle \chi_{\downarrow p}(\alpha_{\downarrow p}) | (-i\partial_{\alpha_{\downarrow p}}) | \chi_{\downarrow p}(\alpha_{\downarrow p}) \rangle] \langle \chi_{\uparrow p}(\alpha_{\uparrow p}) | \tau_y s_y \sigma_0 | \chi_{\downarrow h}(\alpha_{\downarrow h}) \rangle, \tag{S10}
\end{aligned}$$

where we have used the relation $\langle \chi_{\downarrow h}(\alpha_{\downarrow h}) | \partial_{\alpha_{\downarrow h}} \chi_{\downarrow h}(\alpha_{\downarrow h}) \rangle = \langle \chi_{\downarrow p}(\alpha_{\downarrow p}) | \partial_{\alpha_{\downarrow p}} \chi_{\downarrow p}(\alpha_{\downarrow p}) \rangle$ and $\alpha_{\downarrow p} = -\alpha_{\downarrow h}$. So, integrating from edge I to edge II, we get $\langle \chi_{\uparrow p}^{(II)} | \tau_y s_y \sigma_0 | \chi_{\downarrow h}^{(II)} \rangle = e^{-i(\int_0^\pi d\alpha_{\uparrow p} \langle \chi_{\uparrow p}(\alpha_{\uparrow p}) | (-i\partial_{\alpha_{\uparrow p}}) | \chi_{\uparrow p}(\alpha_{\uparrow p}) \rangle + \int_0^\pi d\alpha_{\downarrow p} \langle \chi_{\downarrow p}(\alpha_{\downarrow p}) | (-i\partial_{\alpha_{\downarrow p}}) | \chi_{\downarrow p}(\alpha_{\downarrow p}) \rangle)} \langle \chi_{\uparrow p}^{(I)} | \tau_y s_y \sigma_0 | \chi_{\downarrow h}^{(I)} \rangle = e^{-i\gamma_{pp}} \langle \chi_{\uparrow p}^{(I)} | \tau_y s_y \sigma_0 | \chi_{\downarrow h}^{(I)} \rangle$.

The two-state particle-particle channel Berry phase γ_{pp} can be calculated straightforwardly,

$$\begin{aligned}
\gamma_{pp} &= -i \int_0^\pi d\alpha_{\uparrow p} \langle \chi_{\uparrow p}(\alpha_{\uparrow p}) | \partial_{\alpha_{\uparrow p}} | \chi_{\uparrow p}(\alpha_{\uparrow p}) \rangle - i \int_0^\pi d\alpha_{\downarrow p} \langle \chi_{\downarrow p}(\alpha_{\downarrow p}) | \partial_{\alpha_{\downarrow p}} | \chi_{\downarrow p}(\alpha_{\downarrow p}) \rangle \\
&= -i \int_0^\pi d\alpha_{\uparrow p} \langle \chi_{\uparrow p}(\alpha_{\uparrow p}) | \partial_{\alpha_{\uparrow p}} | \chi_{\uparrow p}(\alpha_{\uparrow p}) \rangle - i \int_\pi^{2\pi} d\alpha_{\downarrow p} \langle \chi_{\downarrow p}(\alpha_{\downarrow p}) | \partial_{\alpha_{\downarrow p}} | \chi_{\downarrow p}(\alpha_{\downarrow p}) \rangle \\
&= -i \int_0^\pi d\alpha_{\uparrow p} \langle \chi_{\uparrow p}(\alpha_{\uparrow p}) | \partial_{\alpha_{\uparrow p}} | \chi_{\uparrow p}(\alpha_{\uparrow p}) \rangle - i \int_\pi^{2\pi} d\alpha_{\uparrow p} \langle \chi_{\uparrow p}(\alpha_{\uparrow p}) | \partial_{\alpha_{\uparrow p}} | \chi_{\uparrow p}(\alpha_{\uparrow p}) \rangle \\
&= -i \int_0^{2\pi} d\alpha_{\uparrow p} \langle \chi_{\uparrow p}(\alpha_{\uparrow p}) | \partial_{\alpha_{\uparrow p}} | \chi_{\uparrow p}(\alpha_{\uparrow p}) \rangle \\
&= \pm \pi \pmod{2\pi}.
\end{aligned} \tag{S11}$$

where we have used the relation $|\chi_{\downarrow}(\alpha_{\downarrow})\rangle = \mathcal{T}'' |\chi_{\uparrow}(\alpha_{\uparrow})\rangle$ and $\alpha_{\uparrow p} = \alpha_{\downarrow p}$. Now it is readily seen that

$$\langle \chi_{\uparrow p}^{(\text{II})} | \tau_y s_y \sigma_0 | \chi_{\downarrow h}^{(\text{II})} \rangle = e^{-i\gamma_{pp}} \langle \chi_{\uparrow p}^{(\text{I})} | \tau_y s_y \sigma_0 | \chi_{\downarrow h}^{(\text{I})} \rangle = -\langle \chi_{\uparrow p}^{(\text{I})} | \tau_y s_y \sigma_0 | \chi_{\downarrow h}^{(\text{I})} \rangle, \tag{S12}$$

which allows the appearance of mass domain wall (intrinsic π junction) at corner B and implies a Majorana Kramers corner modes. The discussion in a more general case [Fig. S1(d)] where the pseudospin polarization isn't fully inverted across the corner (i.e. the joint trajectories of pseudospin of $|\chi_{\uparrow p}\rangle$ and $|\chi_{\downarrow p}\rangle$ are not closed) is the same as that in IA.

II. CONTINUATION CONDITION OF NO MASS DOMAIN WALL

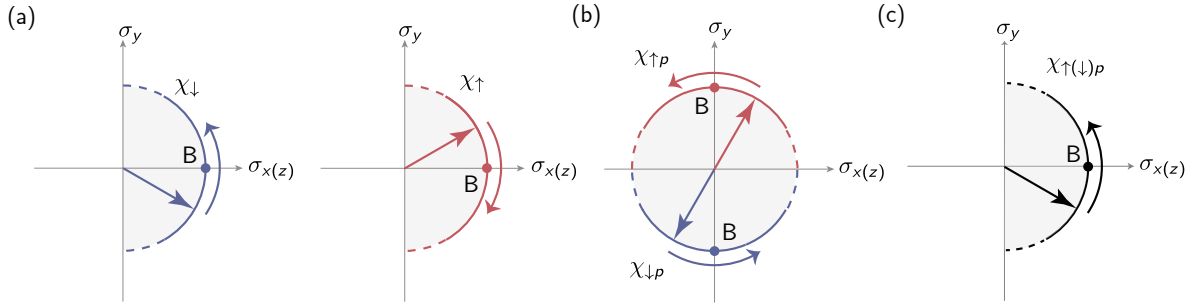


Figure S2. The pseudospin texture in (a) can't guarantee the mass domain wall at corner under a uniform in-plane magnetic field. Solid lines represent the real trajectories while the dashed lines denote the auxiliary paths required by the continuation. Similarly, the pseudospin trajectories in (b) and (c) fail to induce the Majorana Kramers corner modes. The straight red and blue arrows denote the pseudospin vectors for $|\chi_{\uparrow}\rangle$ and $|\chi_{\downarrow}\rangle$, respectively and the straight black arrow represents the coinciding of the two pseudospin vectors.

In this section, we will elucidate when exactly which continuations should be used and discuss the situation where the mass nodes exist on the continuation trajectories when the pseudospin polarization of each spin sector isn't fully reversed across the corner. We have shown that the two-state Berry phase $\gamma_{ph}(\gamma_{pp})$ is well defined when the joint pseudospin trajectory of particle state $|\chi_{\uparrow}\rangle$ and hole state $|\overline{\chi_{\downarrow}}\rangle$ (particle state $|\chi_{\uparrow p}\rangle$ and particle state $|\chi_{\downarrow p}\rangle$) traveling from edge I to II is closed [Fig. 1(c,e,g) in the main text]. Furthermore, this correspondence can be generalized to a more generic case where the joint pseudospin trajectories are non-closed [Fig. 1(d,f,h)]. Hereafter we show how we can find the continuation trajectories in this situation. We take the case in SOTIs for example. Assume that pseudospins of $|\chi_{\uparrow,\downarrow}\rangle$ are confined to $\sigma_x - \sigma_y$ plane, the spin-helical edge states are related by the time-reversal symmetry, so pseudospin textures satisfy $(\langle \sigma_{\uparrow x} \rangle, \langle \sigma_{\uparrow y} \rangle) = (\langle \sigma_{\downarrow x} \rangle, -\langle \sigma_{\downarrow y} \rangle)$. Since the pseudospin of each spin sector isn't fully reversed across the corner [solid lines in Fig. 1(d)], the two-state Berry phase in PH channel is not well defined unless we consider the continuation trajectories [dashed lines in Fig. 1(d)], by which the pseudospins get fully inverted when traveling from edge I to II. Remarkably, the pseudospins in the continuation trajectories are also constrained by time-reversal symmetry. And if we can't find mass node on this auxiliary trajectories, the corner must be mass domain wall.

What will happen when traveling across a corner if mass nodes appear in the continuation trajectories? It is notable that the pseudospin vectors of spin-up state and spin-down state should polarize oppositely in order to obtain a mass node under a uniform in-plane Zeeman field or a conventional s -wave pairing. As shown in Fig. S2(a,b,c), the pseudospin vectors of $|\chi_{\uparrow}\rangle$ and $|\chi_{\downarrow}\rangle$ ($|\chi_{\uparrow p}\rangle$ and $|\chi_{\downarrow h}\rangle$) can polarize oppositely in the dashed lines (continuation trajectories) while the mass terms are always

non-zero and don't change signs in the real trajectories. Therefore, this type of pseudospin textures does not guarantee a mass domain wall at corner and no in-gap corner modes will appear in this special case.

Above consideration can be applied to the concrete models discussed in the main text. For instance, since the pseudospin trajectories around corner B and D in Fig. 2(d) behave like that in Fig. S2(a) and we can only identify the pseudospin vectors polarizing oppositely in the continuation paths, the pseudospin textures does not lead to a mass domain wall at each corner under magnetic field. As a result, one can't observe the appearance of corner modes at B and D. Numerical results shown in Fig. 2(c) confirm our predictions. Similarly, we can also apply this analysis on the corners which can't host the Majorana Kramers corner modes under a conventional s -wave order [Fig. 2]. These examples reflect the validity of our edge geometric phase mechanism.

III. PSEUDOSPIN ANALYSIS FOR THE SECOND-ORDER TOPOLOGICAL INSULATORS

The two prominent models for 2D TIs, the Bernevig-Hughes-Zhang (BHZ) model [1] and the Kane-Mele model [2], both support SOTI phase when subject to an in-plane Zeeman field. We will show the application of edge geometric phase mechanism to these models in detail. Remarkably, the corner modes are pinned at zero energy in the presence of chiral symmetry, while they will be pushed away from zero energy when breaking chiral symmetry. For the sake of simplicity, we take the BHZ model for example to demonstrate this situation. And the Kane-Mele model is assumed to preserve the chiral symmetry.

A. Application to Bernevig-Hughes-Zhang (BHZ) model

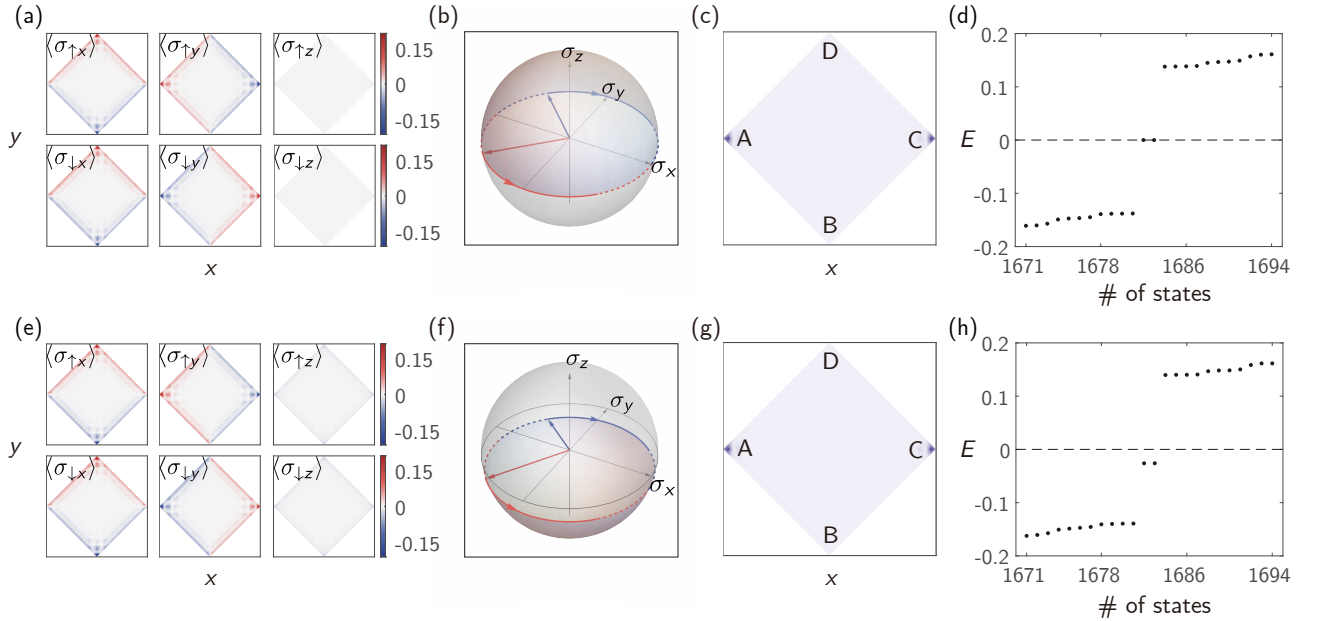


Figure S3. Schematics of the pseudospin analysis for the BHZ model, with parameters $E = 0.3, t_0 = 0.15, m = 2, t = 1, v = 1$. We first show the results in the presence of chiral symmetry. (a) Numerical results of the pseudospin polarizations of the two spin sectors. (b) Trajectories of pseudospin polarizations of spin-up particle (red solid line) and spin-down particle (blue solid line) states traveling from edge BC to CD, with valid continuation (dashed lines). Reversing the direction for the spin-down trajectory gives a complete winding which encircles 2π solid angle. (c) and (d) The distribution of the Dirac corner modes, and the energy level plotted under magnetic field strength $|\mathbf{M}| = 0.2$. As for the case without chiral symmetry, one can refer to (e), (f), (g) and (h).

We elucidate that the corner modes originate from the edge geometric phase in PH channel for the BHZ model, which is similar for the Kane-Mele model. The Hamiltonian is $\mathcal{H}(\mathbf{k}) = \mathcal{H}_{\text{BHZ}}(\mathbf{k}) + \mathcal{H}_Z$, with $\mathcal{H}_Z = M_x s_x + M_y s_y$ and

$$\mathcal{H}_{\text{BHZ}}(\mathbf{k}) = (E - t_0|\mathbf{k}|^2)s_0\sigma_0 + (m - t|\mathbf{k}|^2)s_0\sigma_z + vk_x s_z \sigma_x + vk_y s_0 \sigma_y. \quad (\text{S13})$$

We consider square-shape boundary, with edges terminating the lattice in a tilted way [Fig. 2(a)]. When $\text{sgn } m \text{sgn } t > 0$, for an arbitrary sample edge with normal direction $\hat{\mathbf{x}}_{\perp} = (\cos \theta, \sin \theta)$, assuming a half-infinite sample area $x_{\perp} < 0$, the effective

Hamiltonian can be written as

$$\begin{aligned} \mathcal{H}_{\text{BHZ}}(\mathbf{k}) &= [E - t_0(k_{\parallel}^2 + k_{\perp}^2)]s_0\sigma_0 + [m - t(k_{\parallel}^2 + k_{\perp}^2)]s_0\sigma_z \\ &\quad + v(\sin\theta s_z\sigma_x - \cos\theta s_0\sigma_y)k_{\parallel} + v(\cos\theta s_z\sigma_x + \sin\theta s_0\sigma_y)k_{\perp}. \end{aligned} \quad (\text{S14})$$

$\mathcal{H}_{\text{BHZ}}(\mathbf{k})$ can be separate into two parts: $\mathcal{H}_0(k_{\perp}) = (E - t_0k_{\perp}^2)s_0\sigma_0 + (m - tk_{\perp}^2)s_0\sigma_z + v(\cos\theta s_z\sigma_x + \sin\theta s_0\sigma_y)k_{\perp}$ and $\mathcal{H}_p(k_{\parallel}) = v(\sin\theta s_z\sigma_x - \cos\theta s_0\sigma_y)k_{\parallel}$. The edge states can be obtained by solving the equation $h_{0\uparrow,\downarrow}\psi_{\uparrow,\downarrow}(x_{\perp}) = \epsilon\psi_{\uparrow,\downarrow}(x_{\perp})$: with

$$h_{0\uparrow,\downarrow} = \begin{bmatrix} (E - t_0k_{\perp}^2) + (m - tk_{\perp}^2) & \pm e^{-i\theta}vk_{\perp} \\ \pm e^{i\theta}vk_{\perp} & (E - t_0k_{\perp}^2) - (m - tk_{\perp}^2) \end{bmatrix}, \quad (\text{S15})$$

We replace k_{\perp} with $-i\partial_{x_{\perp}}$ and take the trial function $\psi_{\uparrow}(x_{\perp}) = \begin{bmatrix} \alpha_{\uparrow} \\ \beta_{\uparrow} \end{bmatrix} e^{\lambda x_{\perp}}$ ($\lambda > 0$). So the edge state for spin up takes the form of

$$\psi_{\uparrow}^{\epsilon}(x_{\perp}) = \begin{bmatrix} ie^{-i\theta}v\lambda_1 \\ (E - \epsilon + m) + (t + t_0)\lambda_1^2 \end{bmatrix} \mathcal{N}_1^{\uparrow} e^{\lambda_1 x_{\perp}} + \begin{bmatrix} ie^{-i\theta}v\lambda_2 \\ (E - \epsilon + m) + (t + t_0)\lambda_2^2 \end{bmatrix} \mathcal{N}_2^{\uparrow} e^{\lambda_2 x_{\perp}} \quad (\text{S16})$$

with $\lambda_1 > 0$ and $\lambda_2 > 0$. The boundary condition at $x_{\perp} = 0$ enforces the vanishing of the edge state wavefunction. In the end

$$\psi_{\uparrow}^{\epsilon}(x_{\perp}) = (\mathcal{N}_1^{\uparrow} e^{\lambda_1 x_{\perp}} + \mathcal{N}_2^{\uparrow} e^{\lambda_2 x_{\perp}}) \begin{bmatrix} \sqrt{\frac{t-t_0}{2t}} \\ -ie^{i\theta} \sqrt{\frac{t+t_0}{2t}} \end{bmatrix}. \quad (\text{S17})$$

Similarly, the spinor of edge state for the spin-down sector is $\chi_{\downarrow} = \begin{bmatrix} \sqrt{\frac{t-t_0}{2t}} \\ ie^{-i\theta} \sqrt{\frac{t+t_0}{2t}} \end{bmatrix}$.

Thus the pseudospin polarizations for $|\chi_{\uparrow,\downarrow}\rangle$ are $\langle\sigma_{\uparrow,\downarrow}\rangle = (\frac{\sqrt{t^2-t_0^2}}{t} \sin\theta, \mp \frac{\sqrt{t^2-t_0^2}}{t} \cos\theta, -\frac{t_0}{t})$. Consider the uniform in-plane Zeeman field $\mathcal{H}_Z = M_x s_x + M_y s_y$ and project it onto the subspace spanned by the helical edge states, the effective edge Hamiltonian is $\mathcal{H}_{\text{edge}} = \frac{\sqrt{t^2-t_0^2}}{t} vk_{\parallel} \gamma_z + \sin\theta(-M_x \gamma_y + M_y \gamma_x) - \frac{t_0}{t} \cos\theta(M_x \gamma_x + M_y \gamma_y)$. We first consider the case where \mathcal{H}_{BHZ} has a chiral symmetry, which requires $t_0 = 0$ and leads to $\langle\sigma_{\uparrow,\downarrow}\rangle = (\sin\theta, \mp \cos\theta, 0)$ [Fig. S3(a)]. On the one hand, the trajectories of two pseudospin polarizations across corner C (similar for other corners) are depicted as solid lines in Fig. S3(b), with in-between untraveled paths. We can make a valid continuation [dashed lines in Fig. S3(b)] to concatenate the two trajectories, rendering a two-state π Berry phase in the PH channel. According to the generic theory a mass domain arises at the corner if applying an in-plane Zeeman field, as the mass term $\langle\chi_{\uparrow} | (\mathbf{M} \cdot \mathbf{s}) \sigma_0 | \chi_{\downarrow}\rangle$ is nonzero on the continuation paths, with numerical results shown in Fig. S3(c,d). On the other hand, the effective edge Hamiltonian reads $\mathcal{H}_{\text{edge}} = vk_{\parallel} \gamma_z + \sin\theta(-M_x \gamma_y + M_y \gamma_x)$, which also has a chiral symmetry $\hat{S} = \frac{M_x \gamma_x + M_y \gamma_y}{\sqrt{M_x^2 + M_y^2}}$:

$$\hat{S}^{-1} \mathcal{H}_{\text{edge}} \hat{S} = -\mathcal{H}_{\text{edge}}. \quad (\text{S18})$$

We have known that corner C serves as the mass domain wall which harbors zero-energy corner state. Remarkably, the zero corner mode is also topologically protected due to Eq. S18.

We now consider the case with slight deviation from the chiral symmetry, where t_0 is non-zero but is relatively small compared to t in realistic materials. The pseudospin textures [Fig. S3(e)] $\langle\sigma_{\uparrow,\downarrow}\rangle = (\frac{\sqrt{t^2-t_0^2}}{t} \sin\theta, \mp \frac{\sqrt{t^2-t_0^2}}{t} \cos\theta, -\frac{t_0}{t})$ around corner C are depicted in Fig. S3(f). As we can see, the pseudospin for $|\chi_{\uparrow,\downarrow}\rangle$ are not strictly constrained within $\sigma_x - \sigma_y$ plane, so the two-state Berry phase in PH channel only approximately equals to π . Now the geometric phase doesn't necessitate a sign-change of the edge mass, thus not guaranteeing a mass domain wall. The consequence is that the zero corner modes are not pinned at zero energy, and can be lifted to be of finite energy, but still within the gap [Fig. S3(g) and (h)]. This is justified from the perspective of symmetry: as long as the symmetry-breaking term is not strong enough to drive a phase transition from the HOTI phase to a trivial phase, the edge effective Hamiltonian can be considered as having an approximate chiral symmetry:

$$\hat{S}^{-1} \mathcal{H}_{\text{edge}} \hat{S} \approx -\mathcal{H}_{\text{edge}}. \quad (\text{S19})$$

When the chiral symmetry is broken, the fact that the two-state Berry phase can't quantize to π (even if we made proper continuation to make the pseudospin trajectories closed) in turn illustrates that the edge geometric phase mechanism is complete for understanding the behavior of corner modes.

B. Application to Kane-Mele model

The Kane-Mele model is defined on a honeycomb lattice with pseudospin degree of freedom attributed to the two sublattices,

$$H = \sum_{\langle ij \rangle, \alpha} t c_{i\alpha}^\dagger c_{j\alpha} + \sum_{\langle\langle ij \rangle\rangle, \alpha\beta} it_{\text{SO}} \nu_{ij} s_{\alpha\beta}^z c_{i\alpha}^\dagger c_{j\beta}, \quad (\text{S20})$$

where the first term is the nearest-neighbor hopping, and the second term is the intrinsic SOC for the next-nearest-neighbor hopping, with $\nu_{ij} = +(-)$ if the electron makes a left (right) turn during hopping from site j to i . Different from the models considered in the main text, where the band inversion momentum (Γ point in the Brillouin zone) is coincident with a time-reversal invariant momentum (TRIM), the Kane-Mele model has its band inversion momenta (K, K' point) separate from the TRIM. We take the routine to solve the edge states at the momenta where they are degenerate in energy (i.e. the TRIM), since in this way we can directly diagnose the pseudospin polarization of the edge states. For this reason, in the case of Kane-Mele model, the continuum $\mathbf{k} \cdot \mathbf{p}$ Hamiltonian expanded around K, K' is troublesome to use. Instead, we adopt the lattice approach, which essentially reduces to a quasi-one-dimensional eigenvalue problem for each edge. As an example, we consider the corner-turning process traveling from the lower edge (A) to the lower-right edge C, across the lower-right corner (B).

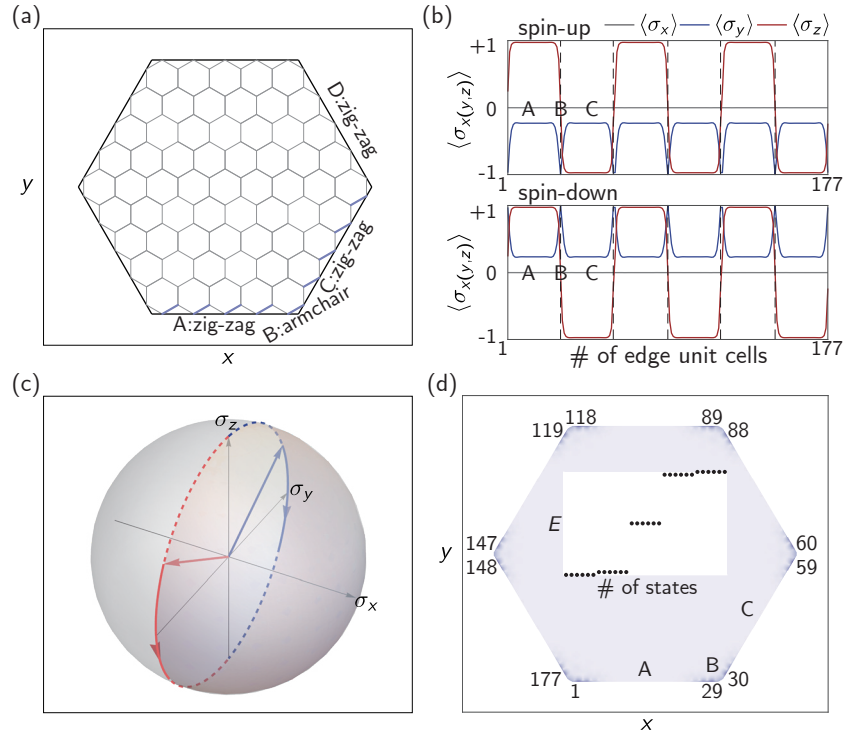


Figure S4. Schematics of the pseudospin analysis for the Kane-Mele model, with parameters $t = 1, t_{\text{so}} = 0.06$. (a) Illustration of lattice configuration and choice for the edge unit cells (colored links). The lower edge (A) and lower-right edge (C) are of zig-zag type boundary condition, while the lower-right corner (B) can be seen as being terminated from an armchair edge. (b) Distribution of the edge states and the energy levels under magnetic field strength $|\mathbf{M}| = 0.2$. (c) Line plot of the pseudospin texture, with edge unit cell indices delineated in (b) at each corner. (d) Trajectories of pseudospin polarizations of spin-up (red solid line) and spin-down (blue solid line) edge states traveling from edge A to C. The continuation (dashed lines) makes the joint trajectory close and encircle half the Bloch sphere.

1. Zig-zag edges

The lower edge (A) is of zig-zag type boundary condition, and the way we choose the edge unit cells is demonstrated as the colored links in Fig. S4(a). In the lattice approach we need to solve the eigenvalue problem $H(k_{\parallel})|\Psi_j(k_{\parallel})\rangle = E(k_{\parallel})|\Psi_j(k_{\parallel})\rangle$, here $\hat{e}_{\parallel} = \hat{e}_x, \hat{e}_{\perp} = \hat{e}_y$. We denote $\mathbf{c}_j(k_{\parallel}) = (c_{j,\uparrow,A}(k_{\parallel}), c_{j,\uparrow,B}(k_{\parallel}), c_{j,\downarrow,A}(k_{\parallel}), c_{j,\downarrow,B}(k_{\parallel}))^T$ and write the tight-binding

Hamiltonian as

$$H(k_{\parallel}) = \sum_j \mathbf{c}_j^{\dagger}(k_{\parallel}) T_0(k_{\parallel}) \mathbf{c}_j(k_{\parallel}) + \mathbf{c}_{j+1}^{\dagger}(k_{\parallel}) T_{+1}(k_{\parallel}) \mathbf{c}_j(k_{\parallel}) + \mathbf{c}_{j-1}^{\dagger}(k_{\parallel}) T_{-1}(k_{\parallel}) \mathbf{c}_j(k_{\parallel}), \quad (\text{S21})$$

with $T_0(k_{\parallel}) = t(1 + \cos k_{\parallel})s_0\sigma_x + t \sin k_{\parallel} s_0\sigma_y - 2t_{so} \sin k_{\parallel} s_z\sigma_z$, $T_{+1}(k_{\parallel}) = \frac{t}{2}e^{-i\frac{k_{\parallel}}{2}}s_0\sigma_x + \frac{it}{2}e^{-i\frac{k_{\parallel}}{2}}s_0\sigma_y + 2t_{so} \sin \frac{k_{\parallel}}{2} s_z\sigma_z$ and $T_{-1}(k_{\parallel}) = \frac{t}{2}e^{i\frac{k_{\parallel}}{2}}s_0\sigma_x - \frac{it}{2}e^{i\frac{k_{\parallel}}{2}}s_0\sigma_y + 2t_{so} \sin \frac{k_{\parallel}}{2} s_z\sigma_z$, and the ansatz $|\Psi_j(k_{\parallel})\rangle = \lambda^{j-1}|\Psi_1(k_{\parallel})\rangle$ ($|\lambda| < 1$) plus the zig-zag boundary condition $|\Psi_{j=1}(k_{\parallel})\rangle = 0$. The edge states are degenerate in energy $E = 0$ at TRIM $k_{\parallel} = \pi$, and the spinor part of the eigenstates solved at this momentum are given by

$$|\chi_{\uparrow}\rangle^{(A)} = \frac{1}{\sqrt{1+\mu}} \begin{bmatrix} 1 \\ 0 \end{bmatrix}_s \otimes \begin{bmatrix} 1 \\ -i\sqrt{\mu} \end{bmatrix}_{\sigma}, \quad |\chi_{\downarrow}\rangle^{(A)} = \frac{1}{\sqrt{1+\mu}} \begin{bmatrix} 0 \\ 1 \end{bmatrix}_s \otimes \begin{bmatrix} 1 \\ i\sqrt{\mu} \end{bmatrix}_{\sigma}, \quad (\text{S22})$$

with $\mu = \left(1 + \frac{t^2}{8t_{so}^2}\right) - \sqrt{\left(1 + \frac{t^2}{8t_{so}^2}\right)^2 - 1}$, and corresponding pseudospin polarizations being $\langle\sigma_{\uparrow,\downarrow}\rangle^{(A)} = \left(0, \mp \frac{2\sqrt{\mu}}{1+\mu}, \frac{1-\mu}{1+\mu}\right)$.

In the same procedure as before but setting $\hat{e}_{\parallel} = \left(\frac{1}{2}, \frac{\sqrt{3}}{2}\right)$, $\hat{e}_{\perp} = \left(-\frac{\sqrt{3}}{2}, \frac{1}{2}\right)$, we can solve out the spinors of the edge states on the lower-right edge (C):

$$|\chi_{\uparrow}\rangle^{(C)} = \frac{1}{\sqrt{1+1/\mu}} \begin{bmatrix} 1 \\ 0 \end{bmatrix}_s \otimes \begin{bmatrix} 1 \\ -i/\sqrt{\mu} \end{bmatrix}_{\sigma}, \quad |\chi_{\downarrow}\rangle^{(C)} = \frac{1}{\sqrt{1+1/\mu}} \begin{bmatrix} 0 \\ 1 \end{bmatrix}_s \otimes \begin{bmatrix} 1 \\ i/\sqrt{\mu} \end{bmatrix}_{\sigma} \quad (\text{S23})$$

and read off their pseudospin polarizations: $\langle\sigma_{\uparrow,\downarrow}\rangle^{(C)} = \left(0, \mp \frac{2\sqrt{\mu}}{1+\mu}, -\frac{1-\mu}{1+\mu}\right)$.

2. Armchair corner

The lower-right corner (B) can be regarded as being terminated from an armchair edge, and within the lattice approach its boundary condition is $|\Psi_{j=1}(k_{\parallel})\rangle = |\Psi_{j=2}(k_{\parallel})\rangle = 0$. In this case, $\hat{e}_{\parallel} = \hat{e}_y$, $\hat{e}_{\perp} = -\hat{e}_x$, and the spinors and pseudospin polarizations of the edge states turn out to be

$$|\chi_{\uparrow}\rangle^{(B)} = \begin{bmatrix} 1 \\ 0 \end{bmatrix}_s \otimes \begin{bmatrix} 1 \\ -i \end{bmatrix}_{\sigma}, \quad |\chi_{\downarrow}\rangle^{(B)} = \begin{bmatrix} 0 \\ 1 \end{bmatrix}_s \otimes \begin{bmatrix} 1 \\ i \end{bmatrix}_{\sigma}; \quad \langle\sigma_{\uparrow}\rangle^{(B)} = (0, -1, 0), \quad \langle\sigma_{\downarrow}\rangle^{(B)} = (0, 1, 0). \quad (\text{S24})$$

3. Pseudospin analysis

The numerical results for the pseudospin of the two edge states are plotted in Fig. S4(b), and their trajectories in the process traveling from edge A to edge C across corner B are depicted as solid arcs in Fig. S4(c). In this case, the pseudospin polarizations lie in the $\sigma_y - \sigma_z$ plane, but the analysis is the same as that in the main text. It's easy to see that the two spinors of pseudospin-1/2 always have a nonzero overlap when the pseudospin vectors are restricted in the regions between the two solid segments, so a continuation can be validly performed [dashed arcs in Fig. S4(c)], rendering a two-state π Berry phase in PH channel. After introducing the in-plane Zeeman field, a mass domain wall must lie in the middle of the solid segments, corresponding to the corner B. With the same analysis, the other five corners are all identified host mass domain walls. The numerical results [Fig. S4(d)] show exact six corner states pinned to the six corners of the sample respectively, confirming our pseudospin analysis.

IV. DERIVATION OF PSEUDOSPIN TEXTURES OF THE SECOND-TYPE QSH PHASE OF THE MATERIAL

In this section, we focus on the second type of QSH phase of the material Au/GaAs(111). As discussed in Ref. [3], effective Hamiltonian of its second type of QSH phase around Γ point in the basis $\psi = (p_{\uparrow+}, p_{\uparrow-}, p_{\downarrow+}, p_{\downarrow-})^T$ can be written as

$$\mathcal{H}_{\text{eff}}(\mathbf{k}) = a_0 s_0 \sigma_0 + a'_0 (k_x^2 + k_y^2) s_0 \sigma_0 + \lambda s_z \sigma_z + a_x (k_x^2 - k_y^2) s_0 \sigma_x + a_y k_x k_y s_0 \sigma_y, \quad (\text{S25})$$

with the coefficients: $a_0 = \varepsilon_p + 3(t_{pp\pi} + t_{pp\sigma})$, $a'_0 = \left[-\frac{3}{4}(t_{pp\pi} + t_{pp\sigma}) + \frac{9t_{sp\sigma}^2/2}{E - (\varepsilon_s + 6t_{ss\sigma})}\right]$ and $a_x = \frac{a_y}{2} = \left[\frac{3}{8}(t_{pp\pi} - t_{pp\sigma}) + \frac{9t_{sp\sigma}^2/2}{E - (\varepsilon_s + 6t_{ss\sigma})}\right]$, where ε_s and ε_p are the on site energy for s and p orbital, respectively. E denote the chemical potential. $t_{ss\sigma}$,

$t_{sp\sigma}$, $t_{pp\sigma}$ and $t_{pp\pi}$ are N.N. hopping parameter, and λ is the SOC strength. Since the effective Hamiltonian in Eq. S25 is written in the basis $(p_x + ip_y, p_x - ip_y)$ and the hybrid orbitals $p_+ = p_x + ip_y$ and $p_- = p_x - ip_y$ are interchanged under time-reversal symmetry $\hat{T}^{-1}p_+\hat{T} = \hat{T}^{-1}(p_x + ip_y)\hat{T} = p_x - ip_y = p_-$. So \hat{T} should be modified to $\hat{T}'' = is_y\sigma_x\mathcal{K}$. And we find that effective Hamiltonian $\mathcal{H}_{\text{eff}}(\mathbf{k})$ of the second type of QSH is time-reversal invariant under this refined operator

$$\hat{T}''^{-1}\mathcal{H}_{\text{eff}}(\mathbf{k})\hat{T}'' = \mathcal{H}_{\text{eff}}(-\mathbf{k}). \quad (\text{S26})$$

We consider an arbitrary sample edge with normal direction $\hat{\mathbf{x}}_{\perp} = (\cos\theta, \sin\theta)$ and assume a half-infinite sample area $x_{\perp} < 0$. The effective Hamiltonian can be written as

$$\begin{aligned} \mathcal{H}_{\text{eff}}(\mathbf{k}) &= a_0\sigma_0s_0 + a'_0(k_{\perp}^2 + k_{\parallel}^2)\sigma_0s_0 + a_x[\cos 2\theta(k_{\perp}^2 - k_{\parallel}^2) - 2\sin 2\theta k_{\perp}k_{\parallel}]\sigma_xs_0 \\ &+ a_y\left[\frac{\sin 2\theta}{2}(k_{\perp}^2 - k_{\parallel}^2) + \cos 2\theta k_{\perp}k_{\parallel}\right]\sigma_ys_0 + \lambda\sigma_zs_z. \end{aligned}$$

We replace $k_{\perp} \rightarrow -i\partial_{\perp}$ and decompose the Hamiltonian as $\mathcal{H}_{\text{eff}} = \mathcal{H}_0 + \mathcal{H}_p$, where $\mathcal{H}_0(-i\partial_{\perp}, k_{\parallel}) = a_0\sigma_0s_0 + a'_0(-\partial_{\perp}^2)\sigma_0s_0 + \lambda\sigma_zs_z + a_x[\cos 2\theta(-\partial_{\perp}^2)]\sigma_xs_0 + a_y\left[\frac{\sin 2\theta}{2}(-\partial_{\perp}^2)\right]\sigma_ys_0$ and $\mathcal{H}_p(-i\partial_{\perp}, k_{\parallel}) = -a_x2\sin 2\theta k_{\parallel}(-i\partial_{\perp})\sigma_xs_0 + a_y\cos 2\theta k_{\parallel}(-i\partial_{\perp})\sigma_ys_0$. Solving the eigenvalue equation $\mathcal{H}_0|\Psi_{\alpha}(x_{\perp})\rangle = \epsilon|\Psi_{\alpha}(x_{\perp})\rangle$ under the boundary conditions $|\Psi_{\alpha}(-\infty)\rangle = 0$, we can obtain two solutions at energy ϵ . And the spinor parts of the two solutions are

$$|\chi_{\uparrow}\rangle = \frac{1}{\mathcal{N}_{\uparrow}} \begin{bmatrix} 1 \\ 0 \end{bmatrix}_s \otimes \begin{bmatrix} \frac{-\lambda a'_0 - \delta}{[\lambda + (a_0 - \epsilon)]a_x} e^{-i2\theta} \\ 1 \end{bmatrix}_{\sigma}, \quad |\chi_{\downarrow}\rangle = \frac{1}{\mathcal{N}_{\uparrow}} \begin{bmatrix} 0 \\ 1 \end{bmatrix}_s \otimes \begin{bmatrix} \frac{-\lambda a'_0 + \delta}{[\lambda - (a_0 - \epsilon)]a_x} e^{-i2\theta} \\ 1 \end{bmatrix}_{\sigma}, \quad (\text{S27})$$

with normalization factors given by $\mathcal{N}_{\uparrow(\downarrow)} = \sqrt{1 + \left(\frac{-\lambda a'_0 \mp \delta}{[\lambda \pm (a_0 - \epsilon)]a_x}\right)^2}$, where $\delta = \sqrt{\lambda^2 a_0'^2 - [\lambda^2 - (a_0 - \epsilon)^2]a_x^2}$. We can set the chemical potential E properly such that $\delta > 0$. It is worth noting that $|\chi_{\uparrow}\rangle$ and $|\chi_{\downarrow}\rangle$ can be related by operator \mathcal{T}'' : $is_y\sigma_x\mathcal{K} \left\{ \frac{1}{\mathcal{N}_{\uparrow}} \begin{bmatrix} 1 \\ 0 \end{bmatrix}_s \otimes \begin{bmatrix} \frac{-\lambda a'_0 - \delta}{[\lambda + (a_0 - \epsilon)]a_x} e^{-i2\theta} \\ 1 \end{bmatrix}_{\sigma} \right\} = \frac{1}{\mathcal{N}_{\uparrow}} \begin{bmatrix} 0 \\ 1 \end{bmatrix}_s \otimes \begin{bmatrix} \frac{-\lambda a'_0 + \delta}{[\lambda - (a_0 - \epsilon)]a_x} e^{-i2\theta} \\ 1 \end{bmatrix}_{\sigma}$. Consequently, pseudospin polarizations of $|\chi_{\uparrow}\rangle$ and $|\chi_{\downarrow}\rangle$ can be expressed as $\langle \chi_{\uparrow, \downarrow} | \boldsymbol{\sigma} | \chi_{\uparrow, \downarrow} \rangle = \left(\frac{2}{\mathcal{N}_{\uparrow}^2} \frac{-\lambda a'_0 \mp \delta}{[\lambda \pm (a_0 - \epsilon)]a_x} \cos 2\theta, \frac{2}{\mathcal{N}_{\uparrow}^2} \frac{-\lambda a'_0 \mp \delta}{[\lambda \pm (a_0 - \epsilon)]a_x} \sin 2\theta, \frac{1}{\mathcal{N}_{\uparrow}^2} \left\{ \frac{-\lambda a'_0 \mp \delta}{[\lambda \pm (a_0 - \epsilon)]a_x} \right\}^2 - 1 \right)$. We notice that $\frac{1}{\mathcal{N}_{\uparrow}^2} \frac{-\lambda a'_0 - \delta}{[\lambda + (a_0 - \epsilon)]a_x} = \frac{1}{\mathcal{N}_{\downarrow}^2} \frac{-\lambda a'_0 + \delta}{[\lambda - (a_0 - \epsilon)]a_x}$, so $\langle \sigma_{\uparrow x} \rangle = \langle \sigma_{\downarrow x} \rangle$, $\langle \sigma_{\uparrow y} \rangle = \langle \sigma_{\downarrow y} \rangle$, $\langle \sigma_{\uparrow z} \rangle = -\langle \sigma_{\downarrow z} \rangle$. This pseudospin textures indicate that the second type of QSH phase can support a π two-state Berry phase in PP channel, which is relevant to our scheme for realizing SOTSC by pure s -wave SC.

In fact, the effective Hamiltonian can be recast into the BdG form:

$$\mathcal{H}_{\text{BdG}} = \begin{bmatrix} \mathcal{H}_{\text{eff}}(\mathbf{k}) & 0 \\ 0 & -\mathcal{H}_{\text{eff}}^*(-\mathbf{k}) \end{bmatrix}, \quad (\text{S28})$$

and the particle-hole degree of freedom τ will involve in the spin-helical edge states:

$$\begin{aligned} |\chi_{\uparrow p}\rangle &= \frac{1}{\mathcal{N}_{\uparrow}} \begin{bmatrix} 1 \\ 0 \end{bmatrix}_{\tau} \otimes \begin{bmatrix} 1 \\ 0 \end{bmatrix}_s \otimes \begin{bmatrix} \frac{-\lambda a'_0 - \delta}{[\lambda + (a_0 - \epsilon)]a_x} e^{-i2\theta} \\ 1 \end{bmatrix}_{\sigma}; |\chi_{\downarrow p}\rangle = \frac{1}{\mathcal{N}_{\downarrow}} \begin{bmatrix} 1 \\ 0 \end{bmatrix}_{\tau} \otimes \begin{bmatrix} 0 \\ 1 \end{bmatrix}_s \otimes \begin{bmatrix} \frac{-\lambda a'_0 + \delta}{[\lambda - (a_0 - \epsilon)]a_x} e^{-i2\theta} \\ 1 \end{bmatrix}_{\sigma} \\ |\chi_{\uparrow h}\rangle &= \frac{1}{\mathcal{N}_{\uparrow}} \begin{bmatrix} 0 \\ 1 \end{bmatrix}_{\tau} \otimes \begin{bmatrix} 1 \\ 0 \end{bmatrix}_s \otimes \begin{bmatrix} \frac{-\lambda a'_0 - \delta}{[\lambda + (a_0 - \epsilon)]a_x} e^{i2\theta} \\ 1 \end{bmatrix}_{\sigma}; |\chi_{\downarrow h}\rangle = \frac{1}{\mathcal{N}_{\downarrow}} \begin{bmatrix} 0 \\ 1 \end{bmatrix}_{\tau} \otimes \begin{bmatrix} 0 \\ 1 \end{bmatrix}_s \otimes \begin{bmatrix} \frac{-\lambda a'_0 + \delta}{[\lambda - (a_0 - \epsilon)]a_x} e^{i2\theta} \\ 1 \end{bmatrix}_{\sigma}. \end{aligned} \quad (\text{S29})$$

Consequently, there are two pairs of spin-helical Majorana edge states compared with the case of QSHI. Then we introduce the uniform s -wave SC $\mathcal{H}_{\text{SC}} = -\Delta_s \tau_y s_y \sigma_0$ to gap out this gapless edge with the superconducting gap written as

$$\begin{aligned} \mathcal{H}_{\text{mass}} &= -\Delta_s \begin{bmatrix} 0 & 0 & 0 & \langle \chi_{\uparrow p} | \tau_y s_y \sigma_0 | \chi_{\downarrow h} \rangle \\ 0 & 0 & \langle \chi_{\uparrow h} | \tau_y s_y \sigma_0 | \chi_{\downarrow p} \rangle & 0 \\ 0 & \langle \chi_{\downarrow p} | \tau_y s_y \sigma_0 | \chi_{\uparrow h} \rangle & 0 & 0 \\ \langle \chi_{\downarrow h} | \tau_y s_y \sigma_0 | \chi_{\uparrow p} \rangle & 0 & 0 & 0 \end{bmatrix} \\ &= -\Delta_s \frac{\mathcal{N}_{\downarrow}}{\mathcal{N}_{\uparrow}} \frac{2}{\mathcal{N}_{\uparrow}^2} \frac{-\lambda a'_0 - \delta}{[\lambda + (a_0 - \epsilon)]a_x} \cos 2\theta s_y \tau_y = \Delta_s \frac{\mathcal{N}_{\downarrow}}{\mathcal{N}_{\uparrow}} \frac{2}{\mathcal{N}_{\downarrow}^2} \frac{-\lambda a'_0 + \delta}{[\lambda - (a_0 - \epsilon)]a_x} \cos 2\theta s_y \tau_y \\ &\propto -\Delta_s \cos 2\theta s_y \tau_y. \end{aligned} \quad (\text{S30})$$

It is easy to see that superconducting mass in Eq. S30 can change sign with the variation of θ , which indicates the formation of mass domain wall. Since both the QSHI and s -wave SC are time-reversal invariant, Majorana Kramer pairs will be bound at the mass domain wall corners. And because the bulk and edges of the system are gapped, eventually we achieve the time-reversal invariant SOTSC. With naturally imprinted particle-hole symmetry of the BdG formalism protecting the topology, the Majorana Kramers pairs are pinned at zero energy without any other symmetry constraint (e.g. chiral symmetry).

V. CRYSTALLINE SYMMETRY ANALYSIS

As stated in the main text, our edge geometric phase mechanism provides a consistent and parallel approach to crystalline symmetry in identifying the higher-order topological phases. We will take the examples in the main text and supplementary materials to demonstrate the consistency in the following.

BHZ model The first example is the BHZ model discussed in the Sec. II with the Hamiltonian

$$\mathcal{H}_{\text{BHZ}}(\mathbf{k}) = (M + t \cos k_x + t \cos k_y) s_0 \sigma_z + v \sin k_x s_x \sigma_x + v \sin k_y s_y \sigma_y. \quad (\text{S31})$$

We have omitted the identity matrix term $(E - t_0 |\mathbf{k}|^2) s_0 \sigma_0$ here for simplicity. Applying an uniform in-plane Zeeman field can drive this QSH phase into a second-order topological insulator (SOTI) phase. As depicted in Fig. S3(c), the mirror symmetry $\hat{M}_y = -i s_x \sigma_z$ is preserved by changing y to $-y$ with the Zeeman field $\mathcal{H}_Z = M_x s_x$ along the x direction. And the total Hamiltonian $\mathcal{H}_{\text{total}} = \mathcal{H}_{\text{BHZ}} + \mathcal{H}_Z$ satisfies $\hat{M}_y \mathcal{H}_{\text{total}}(k_x, k_y) \hat{M}_y^{-1} = \mathcal{H}_{\text{total}}(k_x, -k_y)$. From the perspective of lattice symmetry, $\hat{M}_y = -i s_x \sigma_z$ plays a central role in the second-order topological insulator phase, since it can change the sign of Dirac mass terms of corresponding adjacent edges, which generates a mass domain wall at the corner. In fact, the corner modes of SOTI phase can be essentially attributed to the Jackiw-Rebbi soliton states, and the lattice symmetry determines the positions of Dirac mass domain walls. For example, let's consider an edge that preserves \hat{M}_y and derive the corresponding spin-helical edge states (spinor part): $|\chi_\uparrow\rangle = \frac{1}{\sqrt{2}} \begin{bmatrix} 1 \\ 0 \end{bmatrix}_s \otimes \begin{bmatrix} 1 \\ -i \end{bmatrix}_\sigma$ and $|\chi_\downarrow\rangle = \frac{1}{\sqrt{2}} \begin{bmatrix} 0 \\ 1 \end{bmatrix}_s \otimes \begin{bmatrix} 1 \\ i \end{bmatrix}_\sigma$. Projecting the mirror symmetry operator $\hat{M}_y = -i s_x \sigma_z$ onto the subspace spanned by $|\chi_\uparrow\rangle$ and $|\chi_\downarrow\rangle$:

$$\hat{\mathcal{M}}_y = -i \begin{bmatrix} \langle \chi_\uparrow | s_x \sigma_z | \chi_\uparrow \rangle & \langle \chi_\uparrow | s_x \sigma_z | \chi_\downarrow \rangle \\ \langle \chi_\downarrow | s_x \sigma_z | \chi_\uparrow \rangle & \langle \chi_\downarrow | s_x \sigma_z | \chi_\downarrow \rangle \end{bmatrix} = -i \gamma_x \quad (\text{S32})$$

Then we concentrate on two adjacent edges (BC,CD) around corner C. It is straightforward to see that edge BC and CD can be related by mirror symmetry \hat{M}_y and their Dirac mass terms satisfy: $\hat{\mathcal{M}}_y m_{\text{BC}}(\theta)|_{\theta=-\theta_1} \hat{\mathcal{M}}_y^{-1} = (-i \gamma_x)(M_x \sin \theta_1 \gamma_y)(i \gamma_x) = -M_x \sin \theta_1 \gamma_y = m_{\text{CD}}(\theta)|_{\theta=\theta_1}$. Consequently, mirror symmetry enforces the sign-changing between $m_{\text{BC}}(\theta)|_{\theta=-\theta_1}$ and $m_{\text{CD}}(\theta)|_{\theta=\theta_1}$, for which a topologically protected 0D zero mode must exist at the mass domain wall corner C. Similarly, corner A can also harbor a Dirac zero mode.

Kane-Mele model The tight-binding Hamiltonian of Kane-Mele model reads:

$$\mathcal{H}_{\text{KM}}(\mathbf{k}) = [h_x(\mathbf{k})\sigma_x + h_y(\mathbf{k})\sigma_y]s_0 + h_{\text{SO}}\sigma_z s_z + \lambda\sigma_0 s_y, \quad (\text{S33})$$

where $h_x(\mathbf{k}) = t(1 + 2 \cos 3ak_y/2 \cos \sqrt{3}ak_x/2)$, $h_y(\mathbf{k}) = 2t \sin 3ak_y/2 \cos \sqrt{3}ak_x/2$ and $h_{\text{SO}}(\mathbf{k}) = -2t_{\text{SO}}(\sin \sqrt{3}ak_x - 2 \cos 3ak_y \sin \sqrt{3}ak_x/2)$. when the Zeeman field is along y direction, the mirror symmetry $\hat{M}_y = i\sigma_x s_y$ preserves by changing y to $-y$. As shown in Fig. S4(a), considering an \hat{M}_y -invariant edge (Armchair edge), the spin-helical edge states are $|\chi_\uparrow\rangle = \frac{1}{\sqrt{2}} \begin{bmatrix} 1 \\ 0 \end{bmatrix}_s \otimes \begin{bmatrix} 1 \\ -i \end{bmatrix}_\sigma$ and $|\chi_\downarrow\rangle = \frac{1}{\sqrt{2}} \begin{bmatrix} 0 \\ 1 \end{bmatrix}_s \otimes \begin{bmatrix} 1 \\ i \end{bmatrix}_\sigma$, so we can obtain the mirror symmetry operator projected in edge states subspace: $i\gamma_x$. Additionally, the Dirac mass terms of \hat{M}_y -related edges C and D are $m_D \gamma_y$ and $m_C \gamma_y$. Since $(i\gamma_x)m_C \gamma_y (-i\gamma_x) = -m_C \gamma_y = m_D \gamma_y$, a topologically protected 0D zero mode will be bound at the corner where edges C and D intersect.

Toy model realizing MCKMs We only take the toy model (1) for example. The BdG Hamiltonian is

$$\mathcal{H}_{\text{BdG}}^{(1)} = (M + t \cos k_x + t \cos k_y) s_z \sigma_z \tau_z + v \sin k_x s_0 \sigma_x \tau_0 + v \sin k_y s_0 \sigma_y \tau_z - \Delta_s s_y \sigma_0 \tau_y \quad (\text{S34})$$

It is easy to see that $\hat{M}_x \mathcal{H}_{\text{BdG}}^{(1)}(k_x, k_y) \hat{M}_x^{-1} = \mathcal{H}_{\text{BdG}}^{(1)}(-k_x, k_y)$, where mirror symmetry $\hat{M}_x = i s_x \sigma_y \tau_z$. Considering \hat{M}_x -related two edges AB and BC [Fig. 2(a)], we find that their SC mass terms have opposite signs due to the constraint of mirror symmetry. As a result, corner B (mass domain wall) will bind the Majorana Kramers pair.

Realistic material Au/GaAs(111) Remarkably, it is rather hard to make sure about the lattice symmetries which are preserved in this realistic system shown in Figure. 3, because we made the triangle lattice fitted into a rectangle geometry. We can only say that the continuum Hamiltonian \mathcal{H}_{BdG} [Eq. S28] preserves the effective mirror symmetry $\hat{M}_{\hat{n}=\frac{\sqrt{2}}{2}\hat{x}+\frac{\sqrt{2}}{2}\hat{y}} = -i\tau_z s_z \sigma_z$ with $\hat{M}_{\hat{n}} \mathcal{H}_{\text{total}}^{\text{SC}}(k_x, k_y) \hat{M}_{\hat{n}}^{-1} = \mathcal{H}_{\text{total}}^{\text{SC}}(k_y, -k_x)$ (where $\mathcal{H}_{\text{total}}^{\text{SC}} = \mathcal{H}_{\text{BdG}} + \mathcal{H}_{\text{SC}}$). In fact, edge geometric phase mechanism is more suitable than crystalline symmetry in the present situation for identifying the SC mass domain walls, since considering the boundary pseudospin textures is more convenient than lattice symmetry analysis in such complicated case. Here we can find the SC mass domain walls quickly and accurately by our edge theory.

* YT and ZHH contribute equally to this work.

† Corresponding author: xiongjunliu@pku.edu.cn.

[1] Y. Ren, Z. Qiao, and Q. Niu, Phys. Rev. Lett. **124**, 166804 (2020).

[2] C. Chen, Z. Song, J.-Z. Zhao, Z. Chen, Z.-M. Yu, X.-L. Sheng, and S. A. Yang, Phys. Rev. Lett. **125**, 056402 (2020).

[3] Z. F. Wang, K.-H. Jin, and F. Liu, Nat Commun **7**, 12746 (2016).